Discovery and therapeutic exploitation of Master Regulatory miRNAs in Glioblastoma

Shekhar Saha[#1], Ying Zhang[#1*], Myron K Gilbert Jr[#1], Collin Dube[#1], Farina Hanif[1,2], Elizabeth Qian Xu Mulcahy[1], Sylwia Bednarek[1],Pawel Marcinkiewicz[1], Xiantao Wang[15], Gijung Kwak[3], Kadie Hudson[1], Yunan Sun[1], Manikarna Dinda[5], Tapas Saha[6], Fadila Guessous[1,4], Nichola Cruickshanks[1], Rossymar Rivera Colon[1], Lily Dell'Olio[1], Rajitha Anbu[1], Benjamin Kefas[1,8], Pankaj Kumar[9], Alexander L Klibanov[10], David Schiff[12], Jung Soo Suk[3], Justin Hanes[13], Jamie Mata[14], Markus Hafner[15*] , Roger Abounader[1,11,16*]

Affiliations:

[1]Department of Microbiology, Immunology & Cancer Biology, University of Virginia, Charlottesville, VA 22908, USA.

[2]Department of Biochemistry, Dow International Medical College, Dow University of Health Sciences, OJHA Campus, SUPARCO Road, Karachi 74200, Pakistan.

[3]University of Maryland School of Medicine, 620 W Lexington St, Baltimore, MD 21201, USA.

[4]Laboratory of Onco-Pathology, Biology and Cancer Environment, Faculty of Medicine, University Mohammed 6 of Sciences and Health, Casablanca, Morocco

[5]Department of Biochemistry and Molecular Genetics, University of Virginia School of Medicine, Charlottesville, VA 22908, USA.

[6]Swiss Re, Healthcare, Bengaluru, India.

[7]Bioinformatics Core, University of Virginia School of Medicine, Charlottesville, VA 22908, USA.

[8]Pharmacy, University of Virginia, Charlottesville, VA 22908, USA.

[9]Bioinformatics Core, University of Virginia School of Medicine, Charlottesville, VA 22908, USA.

[10]Cardiovascular Division, University of Virginia, Charlottesville, VA 22908, USA.

[11,12]Neurology, University of Virginia, Charlottesville, VA 22908, USA.

[13]Center for Nanomedicine at the Wilmer Eye Institute, Johns Hopkins University School of Medicine, 733 N Broadway, Baltimore, MD 21205, USA.

[14]Radiology and Medical Imaging, University of Virginia School of Medicine, Charlottesville, Virginia.
[15]National Institute of Arthritis and Musculoskeletal and Skin Diseases, Bethesda, MD 20892, USA.
[16]NCI Designated Comprehensive Cancer Center, University of Virginia, Charlottesville, VA 22908, USA.

# Contributed equally
*Corresponding authors, ra6u@virginia.edu ,markus.hafner@nih.gov, yz5h@virginia.edu

One Sentence Summary: We developed and used new computational, experimental, and therapeutic approaches to identify and therapeutically deliver master regulatory miRNAs to inhibit the growth of glioblastoma, the most common and deadly primary brain tumor.

Abstract

Glioblastoma is a fatal primary malignant brain tumor. Despite therapies involving surgical resection, chemotherapy, and radiation therapy, the average survival for glioblastoma patients remains at approximately 15 months. MicroRNAs (miRNAs) are short noncoding RNA molecules that regulate the expression of the majority of human genes. Numerous genes are concurrently deregulated in glioblastoma. Consequently, molecular monotherapies have failed to achieve improvements in clinical outcomes. Several lines of evidence suggest that simultaneous targeting of several deregulated molecules is required to achieve better therapies. However, the simultaneous targeting of several deregulated oncogenic drivers is severely limited by the fact that the drugs needed to target many deregulated molecules do not currently exist, and because combining several drugs in a clinical setting leads to an exponential increase in toxicity. We hypothesized that we can develop and use miRNA to simultaneously inhibit multiple deregulated genes for more efficacious glioblastoma therapies. The goal of this study was therefore to identify master regulatory microRNAs (miRNAs) and use them to simultaneously target

multiple deregulated molecules for GBM therapy. We defined master regulatory miRNAs as those that target several deregulated genes in glioblastoma. To find master regulatory miRNAs, we first used PAR-CLIP screenings to identify all targets of all miRNAs in glioblastoma cells. We then analyzed TCGA tumor data to determine which of these targets are deregulated in human tumors. We developed and used an algorithm to rank these targets for significance in glioblastoma malignancy based on their magnitude of deregulation, frequency of deregulation, and correlation with patient survival. We then ranked the miRNAs for their capacity of targeting multiple glioblastoma-deregulated genes and therefore the potential to exhibit strong anti-tumor effects when delivered as therapy. Using this strategy, we selected two tumor suppressor master regulatory miRNAs, miR-340, miR-382 and an oncogenic master regulatory miRNA, miR-17. We validated the target genes of the miRNAs and showed that they form part of important glioblastoma regulatory pathways. We then showed that the miRNAs (miR-340 and miR-582) or the miR-17 inhibitor have strong inhibitory effects on glioblastoma cell growth, survival, invasion, stemness and in vivo tumor growth. Ultimately, we developed and successfully tested a new therapeutic approach to delivery miR-340 using MRI guided focused ultrasound and microbubbles (FUS-MB) and special brain penetrating nanoparticles (BPN). This approach resulted in a substantial reduction in tumor volume and prolongation of the survival of glioblastoma-bearing mice and can be translated into clinical trials. We therefore developed and successfully tested a novel strategy to discover and deliver miRNAs for glioblastoma and cancer therapy.

Introduction

Glioblastoma is an aggressive and fatal primary brain cancer that remains a formidable challenge due to its heterogeneity, therapeutic resistance, and invasive nature(*1-3*) . Despite advances in therapies and clinical trials, the standard treatment of maximum surgical resection followed by radiation and temozolomide chemotherapy only extends patient survival to a modest 14.6 months (*4-7*). Next-generation sequencing and single-cell RNA-seq data have revealed the molecular complexities within and between glioblastoma tumors and their microenvironments, contributing to therapeutic resistance and poor outcomes(*8-13*). The Cancer Genome Atlas (TCGA) and other studies

comprehensively analyzed deregulated gene expression in several hundred GBM tumors and described the concurrent deregulation of numerous genes in any single tumor(*14, 15*). Because of this multi-gene deregulation, molecular monotherapies have failed to achieve significant improvements in clinical outcomes. Several lines of evidence suggest that simultaneous targeting of several deregulated molecules is required to achieve better therapies(*16-19*). However, the simultaneous targeting of several deregulated oncogenic drivers using conventional drugs is severely limited by the fact that the drugs needed to target many deregulated molecules do not currently exist, and because combining several drugs in a clinical setting leads to an exponential increase in toxicity(*20*). The goal of this study was to identify master regulatory microRNAs (miRNAs) and use them to simultaneously target multiple deregulated molecules for GBM therapy.

MicroRNAs (miRNAs) are small non-coding RNA molecules that span 19-24 nucleotides. miRNAs play pivotal roles in regulating various cellular processes, including proliferation, invasion, apoptosis, differentiation, and tumorigenesis(*21-23*). MiRNAs exert their effects by binding to the 3'-Untranslated Regions (3'-UTR), coding sequence (CDS), and 5'-Untranslated Regions (5'-UTR) of target genes, facilitating the assembly of argonaute proteins into miRNA-induced silencing complexes (miRISC). The miRISC targets mRNA, leading to either mRNA degradation or translational inhibition(*24-26*). Dysregulation of miRNA expression is a hallmark of various cancer types, where they function as either oncogenes or tumor suppressors (*27-33*). Importantly, because miRNAs do not require full complementarity to inhibit targeted mRNAs, single miRNAs can target and simultaneously inhibit numerous genes(*34-36*).

We reasoned that we could identify master regulatory miRNA and then use them for glioblastoma therapy. We defined master regulatory miRNAs as those that target several deregulated genes in glioblastoma. Using them as therapeutic agents would theoretically be equivalent to using a combination of several drugs that target deregulated glioblastoma driver genes. To find master regulatory miRNAs, we first used PAR-CLIP screenings to identify all targets of all miRNAs in glioblastoma cells. We then analyzed TCGA tumor data to determine which of these targets are deregulated in human tumors.

We developed and used an algorithm to rank these targets for significance in glioblastoma malignancy based on their magnitude of deregulation, frequency of deregulation, and correlation with patient survival. Using an extension of this algorithm, we then ranked the miRNAs for their capacity of targeting multiple glioblastoma genes and therefore exhibit strong anti-tumor effects when delivered as therapy.

A major challenge towards successful miRNA therapy is delivery. Advancements in targeted gene delivery have significantly influenced the field of brain diseases, including brain tumors, stroke, and epilepsy(*37*). Targeted gene therapy offers improved efficacy and reduced toxicity when combined with various therapeutic drugs (*38, 39*). However, the central nervous system's protective blood-brain barrier poses a formidable challenge to drug delivery(*40*). Focused Ultrasound (FUS) presents a noninvasive and reversible approach to transiently open the blood-brain barrier (BBB) in animal models (*41*). This temporary BBB opening facilitates drug delivery in brain tumors and other brain diseases (*42, 43*). Recent clinical studies have successfully used Magnetic Resonance Image-guided FUS with microbubbles to deliver chemotherapeutic drugs to human brains and treat neurodegenerative conditions such as Alzheimer's disease, Parkinson's disease, and amyotrophic lateral sclerosis (*44-48*). This non-invasive method enhances targeted drug delivery precision while minimizing side effects. A second challenge to achieving effective gene therapy distribution in the brain is the extracellular matrix (ECM), a dense and nanoporous network composed of electrostatically charged molecules such as proteoglycans, hyaluronan, and tenascins. These components restrict the diffusion of gene vectors through steric hindrance and adhesive interactions(*49*). To address this problem, Brian P. Mead et. al. developed brain-penetrating nanoparticles (BPN) consisting of poly(beta-amino esters) (PBAE) that are coated with a high density of polyethylene glycol (PEG). This surface modification reduces interactions with the ECM, enhancing the nanoparticles' ability to penetrate the brain tissue and improve their therapeutic efficacy(*50, 51*). A previous report showed that MRI guided Focused Ultrasound has significantly enhanced the delivery of BPNs with diameters ranging from 40-65 nm into the central nervous system (CNS). Moreover, others have successfully used this approach in a Parkinson's disease rat model, delivering BPNs carrying the gene

for glial cell-derived neurotrophic factor (GDNF), which restored several key indicators of neurodegeneration(*52*). Based on the above, we tested in a combined strategy of MRI-guided FUS BPN delivery of miRNAs to overcome the ECM and BBB barriers.

In this study, we integrated PAR-CLIP miRNA target identification with TCGA gene expression and survival data to identify three master regulatory miRNAs that target the maximum number of glioblastoma driver genes: miR-340 and miR-382 as tumor suppressive master regulators and miR-17 as an oncogenic master regulator. We performed extensive functional assays with these master regulatory miRNAs in glioma cell lines and patient-derived stem cells and demonstrated their ability to inhibit cell proliferation, invasion, neurosphere formation, and xenografted tumor growth. Importantly, we also demonstrated that these miRNAs simultaneously targeted multiple glioblastoma-regulating genes in different pathways, decreasing their protein levels. Lastly, we used Magnetic Imaging-guided Focused Ultrasounds (MRgFUS) in conjunction with microbubbles to transiently open the blood-brain barrier, enabling the local delivery of brain penetrating nanoparticle-conjugated miR-340 into the pre-established mouse gliomas. This approach significantly reduced glioma growth and improved mouse survival. This work describes a conceptually new approach to glioblastoma therapy to identify master regulatory miRNAs in glioblastoma and use for the first time clinical grade FUS and nanoparticles to deliver these microRNAs in vivo to inhibit glioblastoma growth. Given the availability of clinical grade FUS and BPN for brain applications, these findings pave the way for novel miRNA therapeutic clinical trials.

Results

Identification of Genome-wide miRNA targets in glioblastoma via PAR-CLIP.

Several online miRNA target prediction tools are available, but they frequently yield false positives and do not capture all relevant targets. To identify master regulatory miRNAs in glioblastoma, we first used Photoactivatable Ribonucleoside-Enhanced Crosslinking and Immunoprecipitation (PAR-CLIP) to experimentally identify genome-wide targets for all miRNAs in glioblastoma cells (**Fig. 1A**). PAR-CLIP was conducted in U87 cells overexpressing Flag-tagged AGO1, AGO2, AGO3 and cells were cultured in presence of

4-thiouridine and the crosslinked RNA fragments bound by AGO1, AGO2, AGO3 were selectively immunoprecipitated with Flag-tag antibody. The purified cross-linked RNA fragments were subjected to reverse transcription, leading to the induction of a T to C mutation at the 4-thiouridine cross-linked sites. The 4-thiouridine incorporation into the nascent RNA is a key component for PAR-CLIP method. The resulting cDNA libraries were then subjected to deep sequencing and comprehensive analysis (**Fig. 1B-C**, **Fig. S1A-E)**. The obtained reads were aligned with the reference human genome, transcriptome and read clusters with T>C signals over background noise to identify miRNA canonical seed sites. The PRalyzer package was employed to assign clusters. Notably, all three AGO PAR-CLIP datasets were collectively analyzed, as we observed a congruent clustered distribution across the samples (**Fig. 1D,E**). A total of 19,483 clusters were obtained from the three AGO PAR-CLIP libraries, with 6,412 for AGO1, 7,007 for AGO2, and 6,064 for AGO3. 4,068 clusters were common across all three AGO samples **(Fig. 1D, Table 1)**. These clusters correspond to 4,583 transcripts, representing approximately 23% of all protein-coding genes, and map to both 3'-UTR and coding regions. A comprehensive list of mRNA targets for AGO1, AGO2, AGO3, along with their associated miRNAs, is provided in **Table 1**. These findings identify all mRNA targets of all miRNAs in glioblastoma. They offer valuable insights into the genome-wide interactions between miRNAs and their targets in glioblastoma cells, illuminating the complex regulatory networks through which miRNAs modulate multiple targets.

Ranking of master regulatory miRNAs based on the importance of their targets in human TCGA tumors.

Having identified all targets of all miRNAs in GBM cells, we next sought to determine the relevance of these targets, and consequently of their targeting miRNAs, to GBM malignancy. This process involved a systematic approach for selecting master regulatory miRNAs, entailing multiple data processing and integration stages outlined in the methods section of this document (**Fig. 1F**). Briefly, we analyzed The Cancer Genome Atlas (TCGA) data for the PAR-CLIP-identified miRNA targets in human tumors. We identified significantly deregulated targets (FDR ≤ 0.05) with a greater than 2-fold change in human tumors using the TCGA database. The targets were then scored based on the magnitude

and frequency of deregulation, as well as their correlation with patient survival, using a Cox coefficient threshold of 0.3 (**Fig. 1G**). We then added the scores for each target, and then added all scores for all targets of each miRNA. The final score for each miRNA represents is potential master regulatory and therapeutic potential because it is a reflection of both the number of its targets and the importance of these target in glioblastoma biology. More details about the scoring algorithms are described in the methods.

Using this computational workflow, we identified several miRNAs that targeted many highly relevant genes that are dysregulated in GBM (**Fig.1H, Fig. S1F** and **Table 1 & 2)**. We designated these miRNAs as master regulators because they can simultaneously target multiple significantly deregulated and biologically relevant genes and inhibit their expressions. This new approach sheds light on the intricate web of miRNA regulation in glioblastoma and contributes to our understanding of its underlying mechanisms. Importantly, it identifies miRNAs that are likely to exert strong therapeutic effects when delivered (tumor suppressive miRNAs targeting numerous oncogenes) or inhibited (oncogenic miRNAs that target numerous tumor suppressors). The comprehensive list of miRNAs, their targets, and their scores can be found in **Table 1 & 2**.

Master regulatory miRNAs miR-340 and miR-382 bind multiple targets and decrease their expression.

Our new approach that integrates PAR-CLIP data and TCGA analyses identified numerous master regulatory miRNAs and their targets. Among these, we focused on two tumor-suppressive miRNAs, miR-340 and miR-382 because these miRNAs had high scores based on the algorithm described above and in the methods, suggesting that they target numerous deregulated oncogenes in glioblastoma. Our analysis determined that the tumor-suppressive master regulatory microRNAs, miR-340 and miR-382, have 300 and 286 targets, respectively. From these, we selected a subset for validation based on their known deregulation in cancers and their widespread expression in multiple glioma samples and patient-derived glioma stem cells. We performed extensive target validation using immunoblot and 3'UTR reporter analyses. To validate the miRNA target repression,

we transfected precursor miR-340 and miR-382 into glioma cell lines A172, U87, U251, as well as patient-derived glioma stem cell lines GSC-34 and GSC-28. These cells were then subjected to immunoblot analysis using antibodies against the selective targets, CD44, TOP2A, MDM2, RHOC, HMGA2, PLAU, and NUSAP1. Overexpression of these miRNAs in various glioma cells, including glioma stem cells, led to a marked reduction in protein levels across all tested glioma cell lines (**Fig. 2A-I**). To determine if miR-340 and miR-382 directly target *CD44, TOP2A, RHOC, MDM2, HMGA2, EGFR, PDGFRA, NUSAP1,* and *PLAU* by binding to their 3' untranslated regions (3'UTRs), we amplified the 3'UTR sequences containing the miR-340 and miR-382 binding sites from genomic DNA and cloned them into the *psiCheck2* luciferase reporter plasmid under the control of the T7 promoter. These 3'UTR luciferase reporter constructs were then transiently transfected into U87 or 293T cells along with either a scrambled control miRNA mimic or mimics of miR-340 or miR-382. Overexpression of miR-340 resulted in a significant 3-fold to 5-fold decrease in luciferase signals for *CD44, TOP2A, RHOC, HMGA2, MDM2, EGFR* and *PDGFRA* ($p < 0.05$). Similarly, miR-382 overexpression led to a significant 3-fold to 5-fold reduction in 3'UTR luciferase signals for PLAU, *CD44, NUSAP1, HMGA2, and MDM2* ($p < 0.05$), compared to scrambled control transfections (**Fig. 2J,K**). These findings provide strong evidence that miR-340 and miR-382 directly bind to their respective 3'UTRs, significantly repressing target gene expression.

miR-17 is an oncogenic master regulatory miRNA in glioma.

We identified miR-17 as one of the top oncogenic master regulatory miRNAs that targets several deregulated tumor suppressor genes in glioblastoma. We validated some of these targets using immunoblot analysis and 3'UTR reporter assays and in several glioma cell lines and patient-derived glioma stem cell lines. Since miR-17 is upregulated in glioblastoma and acts as an oncogene, we inhibited miR-17 by transfecting an anti-miR-17 inhibitor into glioma cell lines (A172, U87, U251) and patient-derived glioma stem cell lines (GSC-28 and GSC-34). We selected specific targets—*ZBTB4, ANKRD11, EHD3,* and *EPHA4*—identified through our PAR-CLIP analysis due to their widespread expression in multiple cell lines. Inhibiting miR-17 resulted in an increased expression of all these targets in both glioblastoma cells and stem cells, indicating that miR-17

suppresses their expression (**Fig. 3A-D**). To confirm that miR-17 directly binds to the 3'UTRs of *ANKRD11, EHD3, EPHA4,* and *ZBTB4,* we conducted a luciferase reporter assay. The 3'UTR regions of these genes, which contain the miR-17 binding sites, were cloned into a *psiCheck2* reporter plasmid. Glioblastoma cells were transfected with either a scrambled anti-miR or an anti-miR-17 inhibitor, along with the luciferase reporter plasmid containing the miR-17 target binding sites. Transfection with the miR-17 inhibitor led to a significant de-repression (increase) in luciferase signals for *ANKRD11, EHD3, EPHA4,* and *ZBTB4* ($p < 0.05$), compared to the scrambled control (**Fig. 3E**). These data show that miR-17 directly binds to and regulates several deregulated mRNAs in glioblastoma.

Master regulatory miRNAs miR-340 and miR-382 regulate multiple pathways in glioblastoma.

After identifying and validating master regulatory miRNAs and their targets, we next investigated their functions. We first performed pathway analyses with the targets of miR-340 and miR-382. We conducted pathway analysis separately with miR-340 and miR-382 targets from PAR-CLIP to understand their general functional regulatory roles. We performed gene ontology (GO) term, Kyoto Encyclopedia of Genes and Genomes (KEGG), and hallmark pathway analysis. The most significant pathways associated with miR-340 were the mitotic cell cycle phase transition, stem cell differentiation, miRNAs in cancer, PI3K-Akt signaling, proteoglycan in cancer, the hallmarks of apoptosis, G2/M-checkpoint and epithelial to mesenchymal transition (**Fig. 4A-C**). The pathways enriched for miR-382 targets were response to hypoxia, signaling pathway associated with miRNA metabolic process, proteoglycan in cancer, miRNAs in cancer, G2/M checkpoint, and epithelial to mesenchymal transition (**Fig.4D-F**). Overall, our results suggest that these miRNAs regulate many different cancer-related pathways and inhibiting them could attenuate glioma growth by inhibiting numerous oncogenic pathways.

Master regulatory miRNAs miR-340 and miR-382 inhibit cell proliferation, invasion, and neurosphere formation in several glioblastoma cell lines.

We then embarked on a thorough assessment of the functional and experimental therapeutic impacts of miR-340 and miR-382. We first quantified their endogenous expression levels in glioblastoma cell lines, GSCs, and banked human tumors including cell lines (A172, T98G, LN18, U251, U87, SNB19), and stem cell lines (GSC-28, GSC-20, GSC-34, GSC-627, GSC-267), as well as patient glioblastoma samples, using quantitative PCR. Normal human astrocytes and normal human cortex were used as a controls. We observed a significant downregulation of miR-340 and miR-382 expression across all cell lines compared to normal human astrocytes, mirroring the pattern observed in patient glioblastoma samples compared to normal brain samples. This consistent downregulation hinted at a potential tumor suppressor role for these miRNAs, which was consistent with our analyses (**Fig. S2A-D**).

Subsequently, we conducted cell proliferation and invasion assays to determine the biological significance of miR-340 and miR-382 *in vitro* across different glioblastoma cell lines. U87 and U251 glioblastoma cells were transfected with either scrambled control miRNA or precursor miR-340 or precursor miR-382, and cell proliferation was assessed through trypan blue staining and live cell counting. Overexpression of precursor miR-340 or miR-382 led to a significant reduction in cell proliferation compared to the scrambled negative control. This effect was time-dependent, with the most pronounced impact observed five-days post miRNA transfection (**Fig. 5A-D**). These results confirm the tumor suppressive nature of these miRNAs in glioma cells. To further investigate the influence of these miRNAs on glioma cell invasion, we performed transwell invasion assays using glioblastoma cell lines A172, U87, and U251. The transwell invasion chambers were pre-coated with collagen IV, one of the abundant extracellular matrix components in the brain. Glioblastoma cell lines were transfected with scrambled control miRNA, or miR-340, or miR-382 precursors before being plated in the transwell chambers with a growth medium containing 0.1% FBS. These cells were allowed to invade through collagen IV layer. Transient overexpression of either miR-340 or miR-382 led to a substantial reduction in glioblastoma cell invasion compared to scrambled negative control miRNA-transfected cells further confirming the tumor suppressive nature of these miRNAs (**Fig.5E-J**).

Glioblastoma contains self-renewing stem cells contributing to tumor initiation and resistance to therapy. To elucidate the effect of the master regulatory miRNAs on the self-renewal property of glioma stem cells, we conducted neurosphere assays using two distinct patient-derived glioma stem cell lines, GSC-34 and GSC-28. We transiently transfected precursor miR-340 or precursor miR-382 or scrambled controls into these glioma stem cells and counted the number of neurospheres seven days post-miRNA transfection. Neurospheres were categorized based on their size under the microscope (10 X magnification) into large, medium, and small groups. Overexpression of miR-340 and miR-382 in these glioma stem cells led to a reduction in the overall number of neurospheres, indicating that these master regulatory miRNAs diminish the self-renewal capabilities of glioblastoma stem cells (**Fig. 5K-N**). The above findings hold promise for the therapeutic use of master regulatory miRNAs in glioblastoma.

Inhibiting oncogenic miR-17 in glioma cells decreased cell proliferation, invasion, and neurosphere formation in a spectrum of glioma cell lines

miR-17 is one of the top oncogenic master regulatory miRNAs identified by our integrated approach. Similar to the tumor suppressive master regulatory miRNAs, we first checked the endogenous expression of miR-17 in multiple glioma and stem cell lines by RT-qPCR **(Fig. S2E,F)**. We observed an increased expression pattern in all glioma and stem cell lines consistent with our algorithm that identified miR-17 as an oncogenic miRNA. Therefore, we performed a series of functional assays with miR-17 in a spectrum of glioma cell lines, including patient-derived glioma stem cells. For the cell proliferation assay, we transfected the inhibitor against miR-17 into multiple glioma cell lines, A172, U87, and U251, and counted the cells on different days. We observed a decrease in cell proliferation after 72 hours of miRNA inhibitor transfection supporting the oncogenic nature of miR-17 in glioma cells **(Fig. 6A-C)**.

Glioblastoma cells often show increased cell invasion by stimulating the degradation of extracellular matrix proteins (Nakada et al., 2003). The transwell cell invasion assay was carried out with anti-miR-17 in glioma cell lines A172, U87, and U251. These glioblastoma cell lines were transfected with either scrambled control or anti-miR-17 and 48 hours after transfection, the invasion assay was carried out with a collagen IV coated transwell

chamber. Inhibition of miR-17 in glioma cell lines A172, U87, and U251 led to a decrease in cell invasion through collagen-coated chambers, which were counted by taking images from five random microscopic fields and quantified with ImageJ software (**Fig. 6D-I)**.

The neurosphere formation assay was performed with glioma stem cell lines GSC-28 and GSC-34. The transfection of glioma stem cell lines with an inhibitor of miR-17 decreases the overall neurosphere formation. We categorized the neurosphere size into three different groups, large, medium, and small, based on the size calculator with ImageJ software. The overall neurosphere number in different categories decreased significantly after miR-17 inhibitor treatment compared to the scrambled control treatment **(Fig. 6J-M)**.

miR-340 and miR-382 inhibit *in vivo* glioblastoma growth.

The impact of miR-340 and miR-382 overexpression in xenografted tumor growth in mice was investigated. The overall experimental strategy is depicted in **Figure 7A.** We transfected $3x10^5$ U87 cells with either a scrambled negative control miRNA (n=7), precursor miR-340 (n=7), precursor miR-382 (n=7), or anti-miR-17 (n=7). The transfected cells were then stereotactically implanted into the striata of 6-week-old immunodeficient mice. Over three weeks, the mice were closely monitored for tumor growth and survival, and MRI images were obtained to visualize the tumors. After three weeks, the scrambled control U87 group exhibited significant tumor growth. In contrast, the groups treated with miR-340 and miR-382 displayed a significant reduction in tumor volume **(Fig. 7B, C)**. Specifically, the scrambled control group reached a tumor volume of (7.58 ± 2.26) mm^3, while the mice bearing miR-340- or miR-382-transfected tumors showed tumor volumes of (4.59 ± 1.44) mm^3 and (2.86 ± 0.9) mm^3, respectively (**Fig. 7C**). The mice implanted with miR-17 inhibitor transfected cells showed a substantial decrease in tumor volume compared to scrambled control **(Fig. 7D,E)**. The scrambled control mice group showed tumor volumes of (5.3 ± 1.94) mm^3, whereas miR-17 inhibitor group exhibited tumor volumes of 0.68 +0.29 mm^3. Collectively, these *in vivo* findings support the use of miR-340, miR-382, the miR-17 inhibitor, or a combination of them as novel therapeutics for glioblastoma.

Therapeutic delivery of nanoparticle-conjugated miR-340 to mice bearing glioblastoma tumors by MRI-guided Focused Ultrasound inhibits tumor growth.

MiRNAs hold immense therapeutic potential, given their capacity to modulate a plethora of cancer-related pathways. However, previous clinical endeavors involving miRNAs encountered formidable obstacles, primarily stemming from the challenges of precise and targeted delivery, which often resulted in systemic side effects and perilous immune responses. We employed a novel noninvasive technique consisting of MRI-guided focused ultrasound (FUS) and microbubbles (MB) (abbreviated as FUS-MB) to facilitate the direct delivery of miRNA into brain tumors in combination with brain-penetrating nanoparticles (BPN) conjugated with lentiviral plasmids encoding for miR-340. This innovative approach (abbreviated FUS-MB-BPN) circumvents the traditional hurdles of miRNA therapeutics, particularly the notorious blood-brain barrier, penetrates the tumor, and delivers cargo loads (miRNAs) to tumor cells. The schematic and overall experimental plan for FUS-MB-BPN are depicted in **Figure 8A-B**. We generated glioblastoma xenografts in immunodeficient mice aged 4-6 weeks, accomplished by intracranial implantation of $3X10^5$ U87 cells into the striata of mice brains. Once the tumors had formed (7-10-days post-injection) we verified the safe and effective opening of the blood-brain barrier. This step was achieved through a meticulously orchestrated combination microbubbles and sonication, resulting in a conspicuous increase in MRI signal intensity surrounding the tumors. This increased signal intensity is attributed to the leakage of the MRI contrast agent, gadobenate dimeglumine, into the brain parenchyma after blood brain barrier opening—an essential validation step for our approach (**Fig. 8C**). To deliver miR-340 into brain tumors, we synthesized poly (beta-amino esters) (PBAE) nanoparticles and coated its surface with polyethelene glycol (PEG). The PEGylated nanoparticles were then mixed with miR-340 plasmid DNA to finally prepared the blood brain penetrating nanoparticles (BPN). We also prepared the BPN particles with control plasmid for our experiment. We extensively characterized this BPN particles because the zeta potential and size of the particles are important parameters for effective blood-brain barrier penetration. The zeta potential and average size of the miR-340 BPN are 70.54 nm and 52.15 nm respectively whereas for control they are 72.51nm and 51.62 nm

respectively. These ~50 nm size nanoparticles are effective for delivering biological molecules within the tumor. The PEGylated formulation combined with PABE polymer produces highly compact, colloidally stable nanoparticles, approximately 50 nm in size, which are exceptionally stable in human plasma(*53*). These BPN nanoparticles were intravenously injected alongside microbubbles (MB), and focused ultrasound (FUS) was applied to the tumor regions to transiently open the blood-brain barrier and facilitate the delivery of the DNA-BPN particles into the tumor. We divided our brain tumor-bearing mice into two cohorts: one receiving nanoparticle conjugated scrambled control miRNA and the other treated with the tumor-suppressive miR-340. Each group consisted of seven mice. The FUS-MB-BPN procedure was then executed. We administered BPN nanoparticles complexed with either control miRNA or miR-340 plasmid DNA via the tail vein after the blood-brain barrier was successfully opened. Subsequent post-MRI images were captured for both the control and miR-340-treated mice, enabling us to assess changes in tumor volume. Delivery of miR-340 by FUS-MB-BPN into the tumors significantly reduced tumor burden compared to the control group. This represents the first successful BPN-FUS-based experimental therapeutic delivery of a miRNA to inhibit tumor growth (**Fig. 8D-E**). Following this promising outcome, we closely monitored the post-FUS-treated mice for survival analysis, which revealed miR-340 delivery into brain tumors significantly extended the survival of these mice compared to those treated with the scrambled control miRNA (**Fig. 8F**). To rule out any toxicity from FUS-MB, we harvested various organs, including the liver, kidney, brain, heart, spleen, lung, lymph nodes and pancreas from treated mice. We then performed H&E staining on these organs, which were analyzed by a Neuropathologist. Our results showed no damage in the liver, kidney, brain, or heart in treated mice compared to the non-treated controls (**Fig. S3A,B**). These findings demonstrate that MRI-guided FUS is a safe and effective strategy for delivering miRNA into brain tumors.

Notably, this study marks a significant development as it is to our knowledge, the first identification of master regulatory miRNAs and their targets using PAR-CLIP in combination with TCGA gene expression and patient survival. Further, we developed and demonstrated for the first time the therapeutic delivery of miRNAs into brain tumors via

FUS-MB-BPN without any apparent associated toxicity. This FUS-MB-BPN approach presents a promising avenue for potential therapeutic applications in glioblastoma treatment, offering a precise and targeted means of delivering miRNA directly into the brain tumors for the simultaneous targeting of multiple oncogenic pathways.

Discussion

Glioblastoma is one of the most heterogeneous, lethal, and aggressive primary brain tumors (*54*). Despite extensive research and clinical trials, many potential therapeutic drugs have faced insurmountable challenges in the context of brain tumors, failing to progress to clinical use primarily due to the formidable obstacles presented by the blood-brain barrier and tumor heterogeneity (*55*). Presently, the mainstay treatment options for brain tumors involve maximal surgical resection followed by a combination of radiation and temozolomide therapy. However, even with these treatments, the median survival for glioblastoma patients remains dishearteningly low, hovering around 15 months (*56*). Adding to the complexity, these primary brain tumors exhibit high invasiveness and resistance to both chemotherapy and radiation therapy, contributing to frequent recurrence in a majority of patients (*57*). Consequently, there exists a compelling need to develop alternative treatment regimens tailored to the unique challenges posed by glioblastoma. MicroRNAs are a class of small noncoding RNA that are deregulated in most cancers including brain tumors, where they function as either oncogenes or tumor suppressors (*58, 59*). Because miRNA do not require full complementary with the targeted mRNA sequences to inhibit gene expression, a single miRNA can target multiple genes and inhibit their expression (*60*). We therefore reasoned that there exist master regulatory miRNAs, which can inhibit multiple deregulated genes in glioblastoma, and that these miRNAs can be used as therapeutic agents/targets, equivalent to using multiple drugs in combination (*61-63*). Combination drug therapies are difficult because many deregulated molecules do not have drugs that target them, and because combining several drugs can lead to exponential increase in toxicity (*64, 65*). The fact that master regulatory miRNA can be used to inhibit multiple targets and pathways simultaneously positions them as potential very efficacious therapeutic molecules for glioblastoma and

cancer therapy. To find master regulatory miRNAs, we first used PAR-CLIP screenings to identify all targets of all miRNAs in glioblastoma cells. We then analyzed TCGA tumor data to determine which of these targets are deregulated in human tumors. We developed and used an algorithm to rank these targets for significance in glioblastoma malignancy based on their magnitude of deregulation, frequency of deregulation, and correlation with patient survival. Using an extension of this algorithm, we then ranked the miRNAs for their capacity of targeting multiple glioblastoma genes and therefore exhibit strong anti-tumor effects when delivered as therapy. This unique approach was invented and developed in our lab and has not been described or published before. It can be applied to any human cancer.

Our approach uncovered numerous miRNAs that had numerous deregulated targets in glioblastoma. We focused on the highly ranked tumor suppressive miR-340 and miR-382 and the oncogenic miR-17. We validated a few of their targets, TOP2A, RHOC, CD44, HMGA2, MDM2 for miR-340 (**Fig. 2A-E**) and CD44, NUSAP1, PLAU, and HMGA2 for miR-382 targets **(Fig. 2F-I)**, and ZBTB4, ANKRD11, EHD3, and EPHA4 for miR-17. The targets we chosen because of their known oncogenic/tumor suppressive roles in multiple cancers (*66-73*). These selected targets were validated across multiple cell lines, including patient-derived glioma stem cell lines using immunoblotting and 3'UTR reporter assays. CD44 is a cell surface adhesion protein, which is highly expressed in many cancers including cancer stem cells and regulates cancer progression and metastasis (*74*). TOP2A has identified as an oncogene in multiple cancers (*67, 75*). TOP2A is overexpressed in pan-cancers and overexpression is correlated with poor prognosis and advanced pathological stages in most cancers (*75*). RhoC is a member of the RhoGTPase family protein which has been shown to involved in cancer cell migration, invasion and metastasis(*76*). All selected targets are deregulated in glioblastoma where they play important roles in regulating malignancy. More targets were identified and validated but are not all discussed in this section due to space limitations.

We then functionally validated the master regulatory miRNAs by performing growth, death, invasion, and differentiation assays as well as in vivo tumor growth assays. These

assays validated the tumor-suppressive (miR-340 and miR-382) or oncogenic (miR-17 potential) effects of the selected master regulatory miRNAs. We found a strong impact through ectopic expression of miR-340, miR-382, or the inhibition of miR-17 in on cell growth, invasion and formation of neurospheres within glioma stem cell lines. We further performed *in vivo* experiments by implanting U87 cells into the striata of immunodeficient nude mice. Overexpression of either miR-340 and miR-382 or inhibition of miR-17 with anti-miR-17 decreased tumor growth substantially. This compelling evidence underscores the potential of these tumor suppressor miRNAs to target a wide array of genes, effectively regulating their expression and modulating oncogenic functions. As illustrated in Figure 4A-F, their impact was pervasive and profound. Given their ability to orchestrate this concerted regulation across multiple pathways, we aptly designated miR-340, miR-382, and miR-17 as "master regulators," and potential therapeutic agents or targets for glioblastoma therapy.

To translate these findings into experimental therapy, we designed and tested a novel approach for the therapeutic delivery of miRNAs to glioblastoma animal models. We prepared miR-340 plasmid DNA complex with brain penetrating nanoparticles and employed MRI-guided focused ultrasound in conjunction with microbubbles to deliver this therapeutic payload directly into the brains of mice harboring gliomas. The result showed a significant reduction in tumor growth compared to negative control miRNA-treated mice. The mice did not exhibit any signs of toxicity. This new noninvasive delivery method represents a pivotal step towards effective and targeted therapeutic interventions; all while mitigating potential side effects. Efficient drug delivery into brain tumors is impeded by the blood-brain barrier(BBB). Utilizing MRI-guided Focused Ultrasound (MRIgFUS) combined with microbubbles provides a noninvasive technique to temporarily open the BBB for delivering therapeutic molecules with brain penetrating nanoparticles at the tumor site, offering both temporal and spatial control (*77-79*). MRgFUS combined with microbubbles has been utilized in multiple studies to deliver therapeutic molecules into brain tumor (*78, 80*). The blood brain barrier inhibits majority of chemotherapeutic drugs delivery into the brain including the chemotherapeutic drug doxorubicin (*81*). The polymeric nanoparticles have many advantages over cationic polymers such as

polyethylenamine (PEI), poly-L-lysine (PLL) nanoparticles because they have more stability in the bloodstream, superior blood-brain barrier crossing potential, increased drug solubility and more drug encapsulated load and controlled drug release make them more suitable for delivering therapeutics when combined with MFgFUS. Among the promising polymers, poly(β-amino esters) (PBABEs) offer a library of nontoxic, biodegradable materials for the compaction of nucleic acids(*82*). In our study we used surface modified PEGylated PBAE nanoparticles which can penetrate brain parenchyma and open BBB efficiently when combined with microbubbles and FUS (*82, 83*). This blood brain penetrating nanoparticles are more diffusive in nature and were able to circulate in the brain at least for 24 hours suggesting they have low adhesive interactions with extracellular matrix that could lead to the clearance or low distribution of this particles in the brain parenchyma. The precision of focused ultrasound transducers enables them to focus on a millimeter scale, accurately targeting only the tumor region.

In conclusion, our study developed and successfully tested novel approaches to identify and therapeutically deliver miRNAs to glioblastoma. This can be translated into clinical trials using the available clinical grade FUS-MB and BPN at our and other institutions. The approaches can also be easily adapted for use in other cancers as well.

Materials and Methods

Computational and experimental workflow for identifying putative master regulatory miRNAs

Our new methodology for identifying key regulatory microRNAs (miRNAs) and their prioritization involved several steps. First, all miRNA mRNA targets were identified through PAR-CLIP **(**described in more detail in the supplementary methods**)**. Argonaute/target gene complexes were collected, the argonaute protein was digested, and the complexed target genes were then sequenced. T/C alignment analysis was used to identify genes with the distinctive mutation that identifies genes that complex with miRNAs. The sequence target fragments were then compared with a list of known miRNA seed sequences using string sequencing matching in R. Specifically, miRNAs that

targeted genes in the 3'-untranslated region were prioritized, while genes with no miRNA matches or matches in the coding or 5'-untranslated regions were filtered out.

Next, we analyzed 166 Glioblastoma Multiforme (GBM) RNA-Seq datasets from The Cancer Genome Atlas (TCGA), which were normalized against 255 normal brain datasets from the Genotype-Tissue Expression (GTEx, n = 255) project using the bowtie and bedtools genomic sequencing alignment packages. For 42,644 genes, these tumor samples were compared to normal using the DESeq2 package in R, revealing genes that were greater than 2-fold up- and downregulated. Prior to downstream analyses, we implemented pre-filtering measures, discarding genes with read counts of less than five reads.

In the third step, the CancerMine database was employed to classify each miRNA target gene as an oncogene (ONC), a tumor suppressor gene (TSG), or neither, using experimentally verified labels from published manuscripts. Using this method, the final curated repository contained 1849 published oncogenes and 1478 published tumor suppressors, a 1.25:1 ratio.

The fourth step involved performing a survival analysis on the significantly deregulated genes from the previous differential expression analysis. Using the R progamming package, survminer, a cox-proportional hazard ratio was determined for each putative target gene.

The fifth step involved filtering out targets that did not have a "consistent" and "significant" survival and deregulation trend. For oncogenic targets, these parameters were determined as a minimum 2-fold increase in expression and a multiple hypothesis adjusted p-value of ≤0.05, coupled with either an inconclusive correlation with survival (cox coefficient between -0.3 and 0.3) or a correlation with poor prognosis (cox coefficient >0.3). Tumor suppressive targets required a minimum 2-fold decrease in expression, an adjusted p-value of ≤0.05, and either an inconclusive correlation with survival or a correlation with good prognosis (cox coefficient <-0.3). Targets that met these criteria were labeled "consistent" and were retained for the next step.

For this sixth step, the retained “consistent” targets were assigned a composite score based on the percentile ranks of their absolute expression and differential expression scores. For example, a target at the 100th percentile would score 1, and at the 0th percentile would score 0, with the highest possible score being 2 for targets at the 100th percentile for both absolute and differential expression.

Subsequently, each miRNA received two scores reflecting the composite scores of their annotated targets: a TSG score from oncogenic targets and an ONC score from tumor suppressive targets. These scores were then ranked by percentile.

In the final analysis, the percentile rank difference between the TSG and ONC scores for each miRNA determined its classification. The ONC percentile rank was subtracted from the TSG rank. A difference exceeding 25% classified a miRNA as a TSG miRNA (TSG>ONC), while a difference below -25% classified it as an ONC miRNA (ONC>TSG). This threshold was derived from the 1.25:1 oncogene enrichment in our Cancermine dataset described in step three of this analysis. For instance, miR-1185, with a TSG score in the 84th percentile and an ONC score in the 12th percentile, was identified as a projected tumor suppressor miRNA (+72% difference). This approach also minimized the emphasis on miRNAs targeting numerous ONC and TSG genes, as they would rank highly in both categories. For example, miR-4709 ranked in the 100th percentile for TSG and 90th percentile for ONC, but would receive "inconclusive" classification by our algorithm, as there is only a 10% score difference in these roles.

Photoactivatable-ribonucleoside-enhanced crosslinking and Immunoprecipitation (PAR-CLIP)

Flag-tagged AGO1, AGO2, AGO3 plasmids were introduced into U87 cells via Lipofectamine 2000 transfection. Following transfection, the cells were subjected to puromycin selection at a concentration of 1 μg/ml for 48 hours to generate stable cell lines. Verification of AGO1, AGO2, AGO3 overexpression was conducted through immunoblot analysis employing AGO1, AGO2, AGO3 antibodies. The PAR-CLIP methodology was implemented and adapted from the previously established protocol (Hafner et al., 2010). Briefly, AGO1, AGO2, AGO3 stable cell lines were cultured

overnight in the presence of 100 µM 4-thiouracil (4SU), to label all cellular nascent RNA. Subsequently, these 4SU-labeled cells were exposed to 365 nm UV light (utilizing a Spectro Linker XL-1500) to effectuate the crosslinking of labeled nascent RNA with RNA binding proteins. Following UV exposure, cells were rinsed twice with 1X PBS, harvested, and lysed using a buffer composed of 50 mM HEPES-KOH (pH 7.5), 150 mM KCl, two mM EDTA (pH 8.0), one mM NaF, 0.5% NP-40, 0.5 mM DTT, and freshly prepared protease inhibitor cocktails. Cell lysates were centrifuged at 15,000Xg for 15 minutes at 4^0C. The supernatant from the lysed cells was subjected to treatment with RNAse T1 at a concentration of 1 U/µl for 15 minutes at room temperature. Subsequently, the Flag-tagged AGO1, AGO2, AGO3 cell lysates' supernatant underwent immunoprecipitation, facilitated by an anti-Flag antibody conjugated to Protein G Dynabeads. The immunoprecipitated material was further subjected to digestion with RNase T1, and the resulting beads were subjected to washing with a high salt wash buffer. The washed beads were re-suspended in a dephosphorylation buffer and treated with calf intestinal alkaline phosphatase for 10 minutes at 37^0C to eliminate phosphate groups from RNA molecules. Next, the dephosphorylated beads were treated with polynucleotide kinase and radioactive [γ-32P]-ATP for 30 minutes at 37^0C to introduce RNA labeling. The protein-RNA complexes were then separated via SDS-PAGE and subsequently electroeluted. These complexes exhibited a migration pattern at around 100 kDa. The electroeluted samples then underwent digestion with proteinase K to release RNA from the complexes, followed by RNA extraction involving an acid phenol/chloroform mixture and ethanol precipitation. The extracted RNA was then converted into cDNA, and adaptor ligation was executed following previously established protocols (*31, 65*). The resulting libraries were sequenced, and the generated short reads were mapped against the human genome hg38, mRNA, and miRNA precursor databases and the clustered sequences were identified. The PAR-CLIP clustered sequences were identified by T to C conversion at the 4-thiouridine cross-linked site. The majority of the clustered sequences were found at the 3'-UTR regions. Finally, the true target sites were determined from the clustered sequences based on the list of input miRNA seed sequences.

In vivo effects of miRNA expression

To assess the impact of miRNA overexpression or inhibition in vivo, a mouse xenograft model was employed. Six-week-old athymic nude mice were obtained from the Jackson Laboratory. U87 cells ($3X10^5$) were seeded in a 6-well plate and transfected with 30 nM of either scrambled negative control miRNA or precursor mir-340, miR-382, or mir-17 inhibitor. After 48 hours of transfection, the cells were trypsinized, counted, and utilized for intracranial injection. All mouse experiments were conducted following the University of Virginia Institutional guidelines. The transfected cell ($3X10^5$) were intracranially injected and stereotactically implanted into the striata of immunodeficient mice, according to a previously established protocol (*66, 67*). After three weeks, MRI imaging was used to visualize and quantify tumor growth. To enhance tumor signal intensity, gadopentetate dimeglumine was intraperitoneally injected. Imaging was conducted using T1-weighted coronal sections with a field size of 2.5 mm × 2.5 mm and a resolution of 256×256 pixels. Osirix lite software was used to calculate tumor volume using MRI tumor images.

Microbubbles preparation

Gas microbubbles were produced in-house using a method previously described (*68*) involving sonication of decafluorobutane gas. The process begins with distearoyl phosphatidylcholine (Lipoid, Germany, or Avanti Polar Lipids, Alabama) and PEG150 monostearate (obtained from Stepan Kessco, Illinois) being dispersed in normal saline at a concentration of 2 mg/ml for each component. This mixture is then sonicated at 20 KHz and 30% power using a Q700 Sonicator (Qsonica, Newton, CT) for 3 minutes to ensure the formation of a submicron micellar dispersion.

To introduce decafluorobutane into the mixture, the headspace of a vial was filled with the gas via a teflon capillary tubing that sparged the gas through the aqueous medium. Sonication was then continued at maximum power for an additional 30 seconds to disperse the gas into the medium and form microbubbles. Following sonication, the sample was allowed to cool and then floated at normal gravity to remove any bubbles larger than 5 μm, in accordance with the guidelines similar to those in(*69*). The prepared microbubbles were then dispensed into individual vials under a decafluorobutane

atmosphere and the vials were stoppered and stored under refrigeration, ensuring they were not frozen. These gas microbubbles are characterized by their neutral nature.

DNA-Brain penetrating nanocomplexes (BPNs) synthesis and characterization

The preparation of BPN formulation was conducted in accordance with the protocol outlined in a previous publication (Mastorakos et al., 2017). In summary, poly(beta-amino esters) (PBAE) and PEGylated PBAE (PEG-PBAE) were synthesized through the conjugation of 1,11-diamino-3,6,9-trioxaundecane (obtained from Millipore Sigma, St. Louis, MO) or 5 kDa methoxy-PEG-N-hydrosuccinimide (mPEG-NHS, 5 kDa, from Sigma-Aldrich) with the acrylate groups on PBAE (sourced from Sigma-Aldrich), respectively. A mixture of PBAE and PEG-PBAE polymers was then prepared at a 3:2 ratio by PBAE amount to create a highly PEGylated surface. For the formulation of DNA-BPN, polymers and nucleic acids were vigorously mixed at a weight ratio of 60 and a volume ratio of 1:5. This mixture was allowed to incubate at room temperature for 30 minutes to facilitate nanoparticle (NP) assembly. Subsequently, the solution was placed into 100 kDa MWCO Amicon Ultra Centrifugal Filters (Millipore Sigma) and centrifuged at 1,000 × g for 15 minutes at 4°C. To remove residual polymers from the DNA-BPN solution, the concentrated DNA-BPNs, with a nucleic acid concentration adjusted to 1 mg/mL, were diluted tenfold with DNase/RNase-Free Distilled Water and re-centrifuged under the same conditions. After undergoing two additional washing steps, the final DNA-BPN solution, with a nucleic acid concentration of 1 mg/mL, was prepared for subsequent in vivo experiments.

MRI-guided Focused Ultrasound (MRIgFUS)

All aspects of animal handling, monitoring, housing, and experiments strictly adhered to the guidelines set forth by the National Institutes of Health and complied with local Institutional Animal Care and Use Committee regulations at the University of Virginia. To establish tumors, immunodeficient mice aged 6-8 weeks were utilized. Specifically, $3X10^5$ U87 cells were intracranially introduced into the striata of immunodeficient mice. After a three-week injection period, MRI-guided focused ultrasound (MRIgFUS) was employed following a well-established protocol, with some modifications(*70*). Briefly, the MRIgFUS

experimental setup featured an MRI-compatible pre-focused eight-element phased array, accompanied by a 1.5 MHz geometrically focused transducer boasting a 25 mm active diameter and a focal ratio of 0.8. These components were interconnected through a phased array generator and a radiofrequency power amplifier. It was connected to an MRI-compatible motorized stage to precisely control the transducer's movements in the rostral-caudal and medial-lateral orientations. Degassed water was introduced into the spherical transducer's membrane to ensure effective coupling between the membrane and the mice's brains. At the same time, acoustic gel was applied to both the inflated membrane and the shaved portion of the mice's skull. These measures prevented the entrapment of air bubbles. For intravenous injections, a catheter was inserted into the mouse's tail. Microbubbles (25 µl/kg body weight) and an MRI contrasting agent, gadobenate dimeglumine (0.1 ml), were administered via this catheter with saline. Subsequently, a series of MRI images were captured. The precise positioning of the mouse's brain relative to the transducer was determined by locating the transducer's position within the MRI space. During sonication and MRI imaging, the mice were positioned in a prone posture. The region of interest (ROI) encompassing the tumor was defined, and sonication was carried out using a 1.5 MHz transducer to induce the opening of the blood-brain barrier around the tumor. MRI images were acquired using a surface coil incorporated into the FUS system. The effectiveness of blood-brain barrier opening was verified by comparing MRI sections before and after sonication. This MRI-guided focused ultrasound approach provided a powerful method for non-invasive modulation of the blood-brain barrier, enabling targeted delivery of therapeutic agents to brain tumors in preclinical models.

Statistical analysis

All the data are represented as mean ± S.E.M. from three independent biological replicates. The P value is calculated by two tailed Student’s t-tests when comparing two groups. P values of < 0.05 were considered statistically significant.

Detailed descriptions of all other methods can be found in the supplementary material

Figure Legends

Figure 1: Identification and prioritization of master regulatory miRNAs in glioblastoma: A) Schematic overview of PAR-CLIP. B) The phosphorimage of SDS-PAGE gel of RNA-Argonaute (Ago) complexes labeled with 5′-32P that were immunoprecipitated with a Flag-tag antibody. The complex is expected to appear near 100 kDa. C) Agarose gel separation of PCR products from AGO1, AGO2, AGO3 PAR-CLIP cDNA libraries. D) A Venn diagram illustrating the overlap in miRNA targets identified with AGO1, AGO2, AGO3. E) Bar graph showing the distribution of identified targets within coding and 3'-UTR regions. F) Diagram depicting the algorithm used for determining master regulatory miRNAs in glioblastoma. G) Volcano plot denoting the significant miRNAs based on Cox Propportional Hazard. H) Classification of miRNAs as oncogenic and tumor-suppressive based on their targets derived from AGO1, AGO2, AGO3 PAR-CLIP.

Figure 2: Validation of miR-340 and miR-382 targets in glioblastoma cells and patient-derived stem cells: A) Glioblastoma cell lines A172, U87, U251, and patient-derived stem cell lines GSC-28 and GSC-34 were transfected with either a scrambled negative control, miR-340, or miR-382. Immunoblots were probed with antibodies against TOP2A (A), RHOC (B), CD44 (C), HMGA2 (D), and MDM2 (E), CD44 (F), NUSAP1 (G), PLAU (H), and HMGA2 (I). GAPDH served as the internal loading control. The data show that miR-340 and miR-382 downregulated protein expression compared to negative controls. J,K) 3'UTR Luciferase activity assay in U87 cells were performed by co-transfecting cells with miR-340 (J) or miR-382 (K) and a psiCheck2 luciferase reporter plasmid containing the 3'-UTR regions of targets CD44, TOP2A, RHOC, HMGA2, MDM2, EGFR, PDGFRA (J), or PLAU, CD44, NUSAP1, HMGA2, and MDM2 (K). The data show that miR-340 and miR-382 decreased luciferase activity for all respective targets compared to controls. Statistical significance was determined using a two-tailed Student's t-test, with * = $P<0.05$.

Figure 3: Validation of miR-17 targets in glioblastoma cells and patient-derived stem cells: A-D) Glioma cell lines A172, U251, GSC-28, and GSC-34 were transfected with a miRNA inhibitor targeting miR-17. Immunoblots were performed with antibodies

against ZBTB4, ANKRD11, EHD3, and EPHA4. GAPDH served as the internal control for loading. The data show that the miR-17 inhibitor increased protein expression compared to negative controls. E) 293T cells were co-transfected with miR-17 inhibitor along with psiCheck2 luciferase reporter plasmid containing the 3'-UTR regions of targets ANKRD11, EHD3, EPHA4 and ZBTB4. The data show that the miR-17 inhibitor increased luciferase activity for all respective 3'UTR targets compared to negative controls 48 hours after the transfection, cells were lysed and luciferase signals were measured. * = P<0.05.

Figure 4: miR-340 and miR-382 regulate different cancer pathways: A-F) Targets identified for miR-340 and miR-382 through PAR-CLIP and The Cancer Genome Atlas (TCGA), were utilized as input for pathway analysis involving Gene Ontology (GO) terms for Biological Processes (BP), Kyoto Encyclopedia of Genes and Genomes (KEGG), and gene set enrichment analysis. The significant pathways are highlighted by red dots.

Figure 5: miR-340 and miR-382 inhibit cell proliferation, invasion, and neurosphere formation in glioblastoma: A-D) Glioblastoma cell lines U87 and U251 were transfected with either a scrambled control, or miR-340, or miR-382. Cell counts were performed at various time points, and miR-340 and miR-382 showed decreased cell growth compared to negative controls. E-J) A172, U87, and U251 cells were transfected with mimic miR-340 and miR-382 and invasion assays were executed. Invaded Images from 5-10 random fields were captured and analyzed using ImageJ software for quantification. miR-340 and miR-382 decreased invasion compared to negative controls K-N) Six-well plates were pre-coated with poly-ornithine, and glioblastoma stem cell lines GSC-28 and GSC-34 were plated and transfected with either scrambled control miRNA, miR-340, or miR-382. Neurosphere images were taken from five distinct fields 72 hours post-transfection and categorized into large, medium, and small using ImageJ software, with quantifications presented in (M, N). miR-340 and miR-382 decreased neurosphere formation compared to negative controls. Data represent mean ± SEM from three independent experiments. * = P<0.05 based on a two-tailed Student's t-test.

Figure 6: Effects of miR-17 inhibition on cell proliferation, invasion, and neurosphere formation in glioblastoma: A-C) A172, U87, and U251 were transfected

with either scrambled control miRNA or a miR-17 inhibitor. Cells were counted 48 hours post-transfection using trypan blue exclusion at various intervals to assess viability. D-I) A172, U87, and U251 cells were transfected with control or miR-17 inhibitor. Invasion assay was carried out and the invaded cells were stained with crystal violet, and images were captured and analyzed using ImageJ software for quantification. J-M) Glioma stem cell lines GSC-28 and GSC-34, plated on poly-ornithine-coated 6-well plates, were transfected with either a scrambled control miRNA or an miR-17 inhibitor. Neurospheres were imaged 72 hours post-transfection in the neurobasal complete growth medium. Images from five different microscopic fields were taken, and neurosphere sizes were categorized into large, medium, and small for quantification using ImageJ software. Data are presented as mean ± SEM from three independent experiments. * = $P<0.05$ based on a two-tailed Student's t-test.

Figure 7: miR-340, miR-382 and miR-17 regulate in vivo tumor growth: A) Schematic overview of the experimental design for tumor implantation and timeline for MRI imaging to assess tumor volume. Each group comprised seven mice for surgery. B-E) U87 cells were transfected with scrambled negative miRNA, miR-340, miR-382, or an inhibitor of miR-17. 48 hours post-transfection, cells were implanted intracranially into the striata of 5-6-week-old immunodeficient mice. Mice were monitored for 3-4 weeks, and MRI imaging was performed to evaluate tumor generation. Representative MRIs and quantification showing that miR-340, miR-382 and anti-miR-17 inhibitor showed reduction in tumor volume compared to Scramble controls. * = $P<0.05$.

Figure 8: Inhibition of in vivo glioma growth through FUS-MB-BPN delivery of miR-340: A) A schematic representation of FUS-MB-BPN-mediated miRNA delivery into mice. B) Overall experimental plan and timeline for FUS-MB-BPN. C) Tumors in mice were sonicated pre and post FUS-MB-BPN, and images were captured to validate blood-brain barrier opening. Microbubbles (MB) were employed to facilitate blood-brain barrier opening. Arrows indicated the tumor location and show dispersion of the contrast demonstrating successful opening of the blood-brain barrier. D,E) Microbubbles were injected through the mice's tail vein, and MRIgFUS was conducted. Upon confirmation of blood-brain barrier opening, BPN conjugated with either scrambled or miR-340 were

injected through the mice's tail vein. The mice were imaged using MRI, and tumor volume shows significant reduction upon delivery of miR-340 compared to Scramble controls at day 15. F) Kaplan Meir survival curve showing miR-340 significantly prolonged survival compared to Scramble control mice. * = $P < 0.05$.

Acknowledgements:

We thank Drs. Jeongwu Lee, Cleveland Clinic and Erik P. Sulman, NYU Langone Health for providing the glioblastoma stem cell lines GSC-28 and GSC-34 respectively. This work is supported by the University of Virginia Bioinformatics Core, Molecular Imaging Core, Advanced Microscopy Facility and Research Histology Core. We would also like to thank dbGAP and TCGA data management team for providing access to the raw RNA-seq data.

Funding:

This study was supported by NIH/NINDS RO1 NS122222, NIH/NCI UO1 CA220841, NIH/NINDS 1R21NS122136, NCI Cancer Center Support Grant P30CA044579, a University of Virginia Comprehensive Cancer Center Pilot Grant, a Schiff Foundation grant, The Ben and Catherine Ivy Foundation, and The Focused Ultrasound Foundation (all to R.A.).

Author Contributions:

Conceptualization: SS, YZ, MKG, CD, RA

Methodology: SS, YZ, MKG, CD, FH, EQXM, PM, XW, GK, NC, RRC, FG, PK, ALK, JSS, JM

Investigation: SS, YZ, MKG, CD, RA

Visualization: SS, YZ, CD, MKG, FH, PM, MD

Funding acquisition: RA

Project administration: RA

Supervision: RA

Writing – original draft: SS and RA

Writing – review & editing: all the authors

Competing interests: The authors declare there are no competing interests.

Data and materials availability:

The PAR-CLIP dataset from the U87 cell line is publicly available on GEO under accession number GSE293517, along with processed data. All relevant data supporting the findings of this study can be obtained from the corresponding author upon reasonable request. Cell lines generated in this study will be made available upon request, subject to a Material Transfer Agreement (MTA). For further information, resource requests, or reagent inquiries, please contact the corresponding author, Roger Abounader (ra6u@virginia.edu).

References

1. A. C. Bellail, S. B. Hunter, D. J. Brat, C. Tan, E. G. Van Meir, Microregional extracellular matrix heterogeneity in brain modulates glioma cell invasion. *The international journal of biochemistry & cell biology* **36**, 1046-1069 (2004).

2. R. Bonavia, M.-d.-M. Inda, W. K. Cavenee, F. B. Furnari, Heterogeneity maintenance in glioblastoma: a social network. *Cancer research* **71**, 4055-4060 (2011).

3. L. B. Hoang-Minh, F. A. Siebzehnrubl, C. Yang, S. Suzuki-Hatano, K. Dajac, T. Loche, N. Andrews, M. Schmoll Massari, J. Patel, K. Amin, Infiltrative and drug-resistant slow-cycling cells support metabolic heterogeneity in glioblastoma. *The EMBO journal* **37**, e98772 (2018).

4. M. Lim, Y. Xia, C. Bettegowda, M. Weller, Current state of immunotherapy for glioblastoma. *Nature reviews Clinical oncology* **15**, 422-442 (2018).

5. R. Stupp, P.-Y. Dietrich, S. O. Kraljevic, A. Pica, I. Maillard, P. Maeder, R. Meuli, R. Janzer, G. Pizzolato, R. Miralbell, Promising survival for patients with newly diagnosed glioblastoma multiforme treated with concomitant radiation plus temozolomide followed by adjuvant temozolomide. *Journal of Clinical Oncology* **20**, 1375-1382 (2002).

6. R. Stupp, M. E. Hegi, W. P. Mason, M. J. Van Den Bent, M. J. Taphoorn, R. C. Janzer, S. K. Ludwin, A. Allgeier, B. Fisher, K. Belanger, Effects of radiotherapy with concomitant and adjuvant temozolomide versus radiotherapy alone on

survival in glioblastoma in a randomised phase III study: 5-year analysis of the EORTC-NCIC trial. *The lancet oncology* **10**, 459-466 (2009).

7. R. Stupp, W. P. Mason, M. J. Van Den Bent, M. Weller, B. Fisher, M. J. Taphoorn, K. Belanger, A. A. Brandes, C. Marosi, U. Bogdahn, Radiotherapy plus concomitant and adjuvant temozolomide for glioblastoma. *New England journal of medicine* **352**, 987-996 (2005).

8. N. A. Charles, E. C. Holland, R. Gilbertson, R. Glass, H. Kettenmann, The brain tumor microenvironment. *Glia* **59**, 1169-1180 (2011).

9. A. P. Patel, I. Tirosh, J. J. Trombetta, A. K. Shalek, S. M. Gillespie, H. Wakimoto, D. P. Cahill, B. V. Nahed, W. T. Curry, R. L. Martuza, Single-cell RNA-seq highlights intratumoral heterogeneity in primary glioblastoma. *Science* **344**, 1396-1401 (2014).

10. A. R. Pine, S. M. Cirigliano, J. G. Nicholson, Y. Hu, A. Linkous, K. Miyaguchi, L. Edwards, R. Singhania, T. H. Schwartz, R. Ramakrishna, Tumor microenvironment is critical for the maintenance of cellular states found in primary glioblastomas. *Cancer discovery* **10**, 964-979 (2020).

11. V. M. Ravi, P. Will, J. Kueckelhaus, N. Sun, K. Joseph, H. Salié, L. Vollmer, U. Kuliesiute, J. von Ehr, J. K. Benotmane, Spatially resolved multi-omics deciphers bidirectional tumor-host interdependence in glioblastoma. *Cancer Cell* **40**, 639-655. e613 (2022).

12. S. Rosenberg, M. Verreault, C. Schmitt, J. Guegan, J. Guehennec, C. Levasseur, Y. Marie, F. Bielle, K. Mokhtari, K. Hoang-Xuan, Multi-omics analysis of primary glioblastoma cell lines shows recapitulation of pivotal molecular features of parental tumors. *Neuro-oncology* **19**, 219-228 (2017).

13. A. T. Yeo, S. Rawal, B. Delcuze, A. Christofides, A. Atayde, L. Strauss, L. Balaj, V. A. Rogers, E. J. Uhlmann, H. Varma, Single-cell RNA sequencing reveals evolution of immune landscape during glioblastoma progression. *Nature Immunology* **23**, 971-984 (2022).

14. C. W. Brennan, R. G. Verhaak, A. McKenna, B. Campos, H. Noushmehr, S. R. Salama, S. Zheng, D. Chakravarty, J. Z. Sanborn, S. H. Berman, R. Beroukhim, B. Bernard, C. J. Wu, G. Genovese, I. Shmulevich, J. Barnholtz-Sloan, L. Zou, R. Vegesna, S. A. Shukla, G. Ciriello, W. K. Yung, W. Zhang, C. Sougnez, T. Mikkelsen, K. Aldape, D. D. Bigner, E. G. Van Meir, M. Prados, A. Sloan, K. L. Black, J. Eschbacher, G. Finocchiaro, W. Friedman, D. W. Andrews, A. Guha, M. Iacocca, B. P. O'Neill, G. Foltz, J. Myers, D. J. Weisenberger, R. Penny, R. Kucherlapati, C. M. Perou, D. N. Hayes, R. Gibbs, M. Marra, G. B. Mills, E. Lander, P. Spellman, R. Wilson, C. Sander, J. Weinstein, M. Meyerson, S.

Gabriel, P. W. Laird, D. Haussler, G. Getz, L. Chin, T. R. Network, The somatic genomic landscape of glioblastoma. *Cell* **155**, 462-477 (2013).

15. N. Cancer Genome Atlas Research, Comprehensive genomic characterization defines human glioblastoma genes and core pathways. *Nature* **455**, 1061-1068 (2008).

16. H. Mao, D. G. LeBrun, J. Yang, V. F. Zhu, M. Li, Deregulated signaling pathways in glioblastoma multiforme: molecular mechanisms and therapeutic targets. *Cancer investigation* **30**, 48-56 (2012).

17. I. Khan, S. Mahfooz, E. B. Elbasan, B. Karacam, M. N. Oztanir, M. A. Hatiboglu, Targeting glioblastoma: The current state of different therapeutic approaches. *Current neuropharmacology* **19**, 1701-1715 (2021).

18. W. Debinski, Drug cocktails for effective treatment of glioblastoma multiforme. *Expert Review of Neurotherapeutics* **8**, 515-517 (2008).

19. A. Shergalis, A. Bankhead, U. Luesakul, N. Muangsin, N. Neamati, Current challenges and opportunities in treating glioblastoma. *Pharmacological reviews* **70**, 412-445 (2018).

20. J. Gagnon, N. G. Dervisis, B. E. Kitchell, Treatment-related toxicities in tumor-bearing cats treated with temozolomide alone or in combination with doxorubicin: a pilot assessment. *Journal of feline medicine and surgery* **14**, 560-565 (2012).

21. S. Lawler, E. A. Chiocca, Emerging functions of microRNAs in glioblastoma. *Journal of neuro-oncology* **92**, 297-306 (2009).

22. R. Rupaimoole, F. J. Slack, MicroRNA therapeutics: towards a new era for the management of cancer and other diseases. *Nature reviews Drug discovery* **16**, 203-222 (2017).

23. I. Vannini, F. Fanini, M. Fabbri, Emerging roles of microRNAs in cancer. *Current opinion in genetics & development* **48**, 128-133 (2018).

24. S. Djuranovic, A. Nahvi, R. Green, miRNA-mediated gene silencing by translational repression followed by mRNA deadenylation and decay. *Science* **336**, 237-240 (2012).

25. H.-o. Iwakawa, Y. Tomari, The functions of microRNAs: mRNA decay and translational repression. *Trends in cell biology* **25**, 651-665 (2015).

26. J. O'Brien, H. Hayder, Y. Zayed, C. Peng, Overview of microRNA biogenesis, mechanisms of actions, and circulation. *Frontiers in endocrinology* **9**, 402 (2018).

27. J. A. Chan, A. M. Krichevsky, K. S. Kosik, MicroRNA-21 is an antiapoptotic factor in human glioblastoma cells. *Cancer Res* **65**, 6029-6033 (2005).

28. X. Zhou, Y. Ren, L. Moore, M. Mei, Y. You, P. Xu, B. Wang, G. Wang, Z. Jia, P. Pu, Downregulation of miR-21 inhibits EGFR pathway and suppresses the growth of human glioblastoma cells independent of PTEN status. *Laboratory investigation* **90**, 144-155 (2010).

29. M. Chen, Z. Medarova, A. Moore, Role of microRNAs in glioblastoma. *Oncotarget* **12**, 1707 (2021).

30. F. Guessous, M. Alvarado-Velez, L. Marcinkiewicz, Y. Zhang, J. Kim, S. Heister, B. Kefas, J. Godlewski, D. Schiff, B. Purow, Oncogenic effects of miR-10b in glioblastoma stem cells. *Journal of neuro-oncology* **112**, 153-163 (2013).

31. B. Kefas, J. Godlewski, L. Comeau, Y. Li, R. Abounader, M. Hawkinson, J. Lee, H. Fine, E. A. Chiocca, S. Lawler, microRNA-7 inhibits the epidermal growth factor receptor and the Akt pathway and is down-regulated in glioblastoma. *Cancer research* **68**, 3566-3572 (2008).

32. Y. Li, F. Guessous, Y. Zhang, C. DiPierro, B. Kefas, E. Johnson, L. Marcinkiewicz, J. Jiang, Y. Yang, T. D. Schmittgen, MicroRNA-34a inhibits glioblastoma growth by targeting multiple oncogenes. *Cancer research* **69**, 7569-7576 (2009).

33. J. C. Pang, W. K. Kwok, Z. Chen, H. K. Ng, Oncogenic role of microRNAs in brain tumors. *Acta neuropathologica* **117**, 599-611 (2009).

34. M. Selbach, B. Schwanhäusser, N. Thierfelder, Z. Fang, R. Khanin, N. Rajewsky, Widespread changes in protein synthesis induced by microRNAs. *Nature* **455**, 58-63 (2008).

35. D. Baek, J. Villén, C. Shin, F. D. Camargo, S. P. Gygi, D. P. Bartel, The impact of microRNAs on protein output. *Nature* **455**, 64-71 (2008).

36. A. Wilczynska, M. Bushell, The complexity of miRNA-mediated repression. *Cell Death & Differentiation* **22**, 22-33 (2015).

37. J. Sun, S. Roy, Gene-based therapies for neurodegenerative diseases. *Nature neuroscience* **24**, 297-311 (2021).

38. G. U. Dachs, G. J. Dougherty, I. J. Stratford, D. J. Chaplin, Targeting gene therapy to cancer: a review. *Oncology Research Featuring Preclinical and Clinical Cancer Therapeutics* **9**, 313-325 (1997).

39. J. A. Roth, R. J. Cristiano, Gene therapy for cancer: what have we done and where are we going? *Journal of the National Cancer Institute* **89**, 21-39 (1997).

40. R. K. Upadhyay, Drug delivery systems, CNS protection, and the blood brain barrier. *BioMed research international* **2014**, (2014).

41. J. J. Choi, M. Pernot, S. A. Small, E. E. Konofagou, Noninvasive, transcranial and localized opening of the blood-brain barrier using focused ultrasound in mice. *Ultrasound in medicine & biology* **33**, 95-104 (2007).

42. A. Burgess, K. Shah, O. Hough, K. Hynynen, Focused ultrasound-mediated drug delivery through the blood–brain barrier. *Expert review of neurotherapeutics* **15**, 477-491 (2015).

43. D. McMahon, M. A. O'Reilly, K. Hynynen, Therapeutic agent delivery across the blood–brain barrier using focused ultrasound. *Annual Review of Biomedical Engineering* **23**, 89-113 (2021).

44. H. Estrada, J. Robin, A. Özbek, Z. Chen, A. Marowsky, Q. Zhou, D. Beck, B. Le Roy, M. Arand, S. Shoham, High-resolution fluorescence-guided transcranial ultrasound mapping in the live mouse brain. *Science Advances* **7**, eabi5464 (2021).

45. P. S. Fishman, J. M. Fischell, Focused ultrasound mediated opening of the blood-brain barrier for neurodegenerative diseases. *Frontiers in Neurology* **12**, 749047 (2021).

46. C. Gasca-Salas, B. Fernández-Rodríguez, J. A. Pineda-Pardo, R. Rodríguez-Rojas, I. Obeso, F. Hernández-Fernández, M. Del Álamo, D. Mata, P. Guida, C. Ordás-Bandera, Blood-brain barrier opening with focused ultrasound in Parkinson's disease dementia. *Nature communications* **12**, 779 (2021).

47. M. Kinoshita, N. McDannold, F. A. Jolesz, K. Hynynen, Targeted delivery of antibodies through the blood-brain barrier by MRI-guided focused ultrasound. *Biochemical and biophysical research communications* **340**, 1085-1090 (2006).

48. J. M. Wasielewska, A. R. White, Focused ultrasound-mediated drug delivery in humans–A path towards translation in neurodegenerative diseases. *Pharmaceutical Research* **39**, 427-439 (2022).

49. E. Nance, K. Timbie, G. W. Miller, J. Song, C. Louttit, A. L. Klibanov, T.-Y. Shih, G. Swaminathan, R. J. Tamargo, G. F. Woodworth, Non-invasive delivery of stealth, brain-penetrating nanoparticles across the blood− brain barrier using MRI-guided focused ultrasound. *Journal of controlled release* **189**, 123-132 (2014).

50. E. Nance, C. Zhang, T.-Y. Shih, Q. Xu, B. S. Schuster, J. Hanes, Brain-penetrating nanoparticles improve paclitaxel efficacy in malignant glioma following local administration. *ACS nano* **8**, 10655-10664 (2014).

51. B. P. Mead, P. Mastorakos, J. S. Suk, A. L. Klibanov, J. Hanes, R. J. Price, Targeted gene transfer to the brain via the delivery of brain-penetrating DNA nanoparticles with focused ultrasound. *Journal of Controlled Release* **223**, 109-117 (2016).

52. C.-H. Fan, C.-Y. Ting, C. Y. Lin, H.-L. Chan, Y.-C. Chang, Y.-Y. Chen, H.-L. Liu, C.-K. Yeh, Noninvasive, targeted and non-viral ultrasound-mediated GDNF-plasmid delivery for treatment of Parkinson's disease. *Scientific reports* **6**, 19579 (2016).

53. P. Mastorakos, A. L. Da Silva, J. Chisholm, E. Song, W. K. Choi, M. P. Boyle, M. M. Morales, J. Hanes, J. S. Suk, Highly compacted biodegradable DNA nanoparticles capable of overcoming the mucus barrier for inhaled lung gene therapy. *Proceedings of the National Academy of Sciences* **112**, 8720-8725 (2015).

54. F. Hanif, K. Muzaffar, K. Perveen, S. M. Malhi, S. U. Simjee, Glioblastoma multiforme: a review of its epidemiology and pathogenesis through clinical presentation and treatment. *Asian Pacific journal of cancer prevention: APJCP* **18**, 3 (2017).

55. O. Van Tellingen, B. Yetkin-Arik, M. De Gooijer, P. Wesseling, T. Wurdinger, H. De Vries, Overcoming the blood–brain tumor barrier for effective glioblastoma treatment. *Drug Resistance Updates* **19**, 1-12 (2015).

56. R. Stupp, M. Mayer, R. Kann, W. Weder, A. Zouhair, D. C. Betticher, A. D. Roth, R. A. Stahel, S. B. Majno, S. Peters, Neoadjuvant chemotherapy and radiotherapy followed by surgery in selected patients with stage IIIB non-small-cell lung cancer: a multicentre phase II trial. *The lancet oncology* **10**, 785-793 (2009).

57. Y. P. Ramirez, J. L. Weatherbee, R. T. Wheelhouse, A. H. Ross, Glioblastoma multiforme therapy and mechanisms of resistance. *Pharmaceuticals* **6**, 1475-1506 (2013).

58. T. Dalmay, D. Edwards, MicroRNAs and the hallmarks of cancer. *Oncogene* **25**, 6170-6175 (2006).

59. B. Zhang, X. Pan, G. P. Cobb, T. A. Anderson, microRNAs as oncogenes and tumor suppressors. *Developmental biology* **302**, 1-12 (2007).

60. M. Peter, Targeting of mRNAs by multiple miRNAs: the next step. *Oncogene* **29**, 2161-2164 (2010).

61. D. Ghosh, S. Nandi, S. Bhattacharjee, Combination therapy to checkmate Glioblastoma: clinical challenges and advances. *Clinical and translational medicine* **7**, 33 (2018).

62. M. Houweling, A. Giczewska, K. Abdul, N. Nieuwenhuis, A. Küçükosmanoglu, K. Pastuszak, R. C. Buijsman, P. Wesseling, L. Wedekind, D. Noske, Screening of predicted synergistic multi-target therapies in glioblastoma identifies new treatment strategies. *Neuro-oncology advances* **5**, vdad073 (2023).

63. P. Jiang, R. Mukthavavam, Y. Chao, I. S. Bharati, V. Fogal, S. Pastorino, X. Cong, N. Nomura, M. Gallagher, T. Abbasi, Novel anti-glioblastoma agents and therapeutic combinations identified from a collection of FDA approved drugs. *Journal of translational medicine* **12**, 1-13 (2014).

64. R. B. Mokhtari, T. S. Homayouni, N. Baluch, E. Morgatskaya, S. Kumar, B. Das, H. Yeger, Combination therapy in combating cancer. *Oncotarget* **8**, 38022 (2017).

65. C. D. Scripture, W. D. Figg, Drug interactions in cancer therapy. *Nature Reviews Cancer* **6**, 546-558 (2006).

66. K. L. Mooney, W. Choy, S. Sidhu, P. Pelargos, T. T. Bui, B. Voth, N. Barnette, I. Yang, The role of CD44 in glioblastoma multiforme. *Journal of Clinical Neuroscience* **34**, 1-5 (2016).

67. L. Uusküla-Reimand, M. D. Wilson, Untangling the roles of TOP2A and TOP2B in transcription and cancer. *Science advances* **8**, eadd4920 (2022).

68. K. Al-Kuraya, H. Novotny, P. Bavi, A. K. Siraj, S. Uddin, A. Ezzat, N. Al Sanea, F. Al-Dayel, H. Al-Mana, S. S. Sheikh, HER2, TOP2A, CCND1, EGFR and C-MYC oncogene amplification in colorectal cancer. *Journal of clinical pathology* **60**, 768-772 (2007).

69. Y. Zhao, H. Yu, W. Hu, The regulation of MDM2 oncogene and its impact on human cancers. *Acta Biochim Biophys Sin* **46**, 180-189 (2014).

70. K. L. van Golen, Z.-F. Wu, X. T. Qiao, L. W. Bao, S. D. Merajver, RhoC GTPase, a novel transforming oncogene for human mammary epithelial cells that partially recapitulates the inflammatory breast cancer phenotype. *Cancer research* **60**, 5832-5838 (2000).

71. B. Mansoori, A. Mohammadi, H. J. Ditzel, P. H. Duijf, V. Khaze, M. F. Gjerstorff, B. Baradaran, HMGA2 as a critical regulator in cancer development. *Genes* **12**, 269 (2021).

72. G. Chen, J. Sun, M. Xie, S. Yu, Q. Tang, L. Chen, PLAU promotes cell proliferation and epithelial-mesenchymal transition in head and neck squamous cell carcinoma. *Frontiers in genetics* **12**, 651882 (2021).

73. Y. Hu, Z. Xue, C. Qiu, Z. Feng, Q. Qi, J. Wang, W. Jin, Z. Zhong, X. Liu, W. Li, Knockdown of NUSAP1 inhibits cell proliferation and invasion through downregulation of TOP2A in human glioblastoma. *Cell Cycle* **21**, 1842-1855 (2022).

74. Y. Yan, X. Zuo, D. Wei, Concise review: emerging role of CD44 in cancer stem cells: a promising biomarker and therapeutic target. *Stem cells translational medicine* **4**, 1033-1043 (2015).

75. X. Wang, J. Wang, L. Lyu, X. Gao, Y. Cai, B. Tang, Oncogenic role and potential regulatory mechanism of topoisomerase IIα in a pan-cancer analysis. *Scientific Reports* **12**, 11161 (2022).

76. F. M. Vega, G. Fruhwirth, T. Ng, A. J. Ridley, RhoA and RhoC have distinct roles in migration and invasion by acting through different targets. *Journal of Cell Biology* **193**, 655-665 (2011).

77. P.-Y. Chen, H.-Y. Hsieh, C.-Y. Huang, C.-Y. Lin, K.-C. Wei, H.-L. Liu, Focused ultrasound-induced blood–brain barrier opening to enhance interleukin-12 delivery for brain tumor immunotherapy: a preclinical feasibility study. *Journal of translational medicine* **13**, 1-12 (2015).

78. L. Lamsam, E. Johnson, I. D. Connolly, M. Wintermark, M. H. Gephart, A review of potential applications of MR-guided focused ultrasound for targeting brain tumor therapy. *Neurosurgical focus* **44**, E10 (2018).

79. S.-K. Wu, C.-L. Tsai, Y. Huang, K. Hynynen, Focused ultrasound and microbubbles-mediated drug delivery to brain tumor. *Pharmaceutics* **13**, 15 (2020).

80. J. Ishida, S. Alli, A. Bondoc, B. Golbourn, N. Sabha, K. Mikloska, S. Krumholtz, D. Srikanthan, N. Fujita, A. Luck, MRI-guided focused ultrasound enhances drug delivery in experimental diffuse intrinsic pontine glioma. *Journal of Controlled Release* **330**, 1034-1045 (2021).

81. L. H. Treat, N. McDannold, Y. Zhang, N. Vykhodtseva, K. Hynynen, Improved anti-tumor effect of liposomal doxorubicin after targeted blood-brain barrier disruption by MRI-guided focused ultrasound in rat glioma. *Ultrasound in medicine & biology* **38**, 1716-1725 (2012).

82. J. Kim, S. K. Mondal, S. Y. Tzeng, Y. Rui, R. Al-Kharboosh, K. K. Kozielski, A. G. Bhargav, C. A. Garcia, A. Quiñones-Hinojosa, J. J. Green, Poly (ethylene

glycol)–poly (beta-amino ester)-based nanoparticles for suicide gene therapy enhance brain penetration and extend survival in a preclinical human glioblastoma orthotopic xenograft model. *ACS biomaterials science & engineering* **6**, 2943-2955 (2020).

83. R. J. Fields, C. J. Cheng, E. Quijano, C. Weller, N. Kristofik, N. Duong, C. Hoimes, M. E. Egan, W. M. Saltzman, Surface modified poly (β amino ester)-containing nanoparticles for plasmid DNA delivery. *Journal of controlled release* **164**, 41-48 (2012).

Supplementary methods

Cell culture and transfection

All glioblastoma cell lines used in this study were procured from the American Type Culture Collection (ATCC). Specifically, U87 cells were cultured and maintained in Minimal Essential Medium (MEM) supplemented with one mM sodium pyruvate, one mM non-essential amino acids (NEAA), 10 ml of 7.5% sodium bicarbonate, 1% penicillin/streptomycin, and 10% fetal bovine serum. A172 and 293T cells were cultured in DMEM high glucose medium supplemented with 1% penicillin/streptomycin and 10% fetal bovine serum. Glioblastoma stem cells, GSC-34, we from Cleveland Clinic, and GSC-28 were obtained from MD Anderson Cancer Center. These stem cells were cultured following a previously published protocol (*25*). The culture medium for stem cells consisted of 2.5 ml of N-2 (0.5X), 5 ml of B27 (0.5X), 50 ng/ml EGF, 50 ng/ml FGF, 0.5 mM glutamine, and 1% penicillin/streptomycin. Regular maintenance included dissociation using an accutase solution when the neurospheres reached a specific size. The primary astrocytes were from Lonza Bisoscience and were cultured in growth medium kit from Lonza Bioscience. All cells were cultured at 37°C in a humidified incubator with a 5% CO2 atmosphere to maintain cell viability. Both glioblastoma and GSCs were transiently transfected with either 30 nM of a scrambled negative control miRNA, target-specific mimic primary miRNA, or 30-50 nM of a miRNA inhibitor, using the RNAiMax reagent. Following transfection, the culture medium was replaced with a complete growth medium after 6-8 hours. Subsequently, cells were harvested 48 hours post-transfection for various analyses, including RNA isolation, cDNA synthesis, qPCR, and cell lysate preparation for immunoblot analysis to validate miRNA targets.

3’UTR reporter assay

We conducted luciferase reporter assays to investigate miRNA interactions with specific target genes according to the previously published literature (*25*). First, we PCR amplified the 3’-UTRs (3' untranslated regions) targeted by miR-340, miR-382 and miR-17 from genomic DNA. These amplified sequences were then cloned into the psiCheck2 vector,

which had been digested with BamH1 and Not1 restriction enzymes. The primers used for amplifying genomic DNA are shown in **Supplementary Table 1**. All reporter plasmids were subjected to Sanger sequencing and verification to ensure sequence accuracy. for the reporter assay, we co-transfected the primary miRNAs along with 1 µg of the psiCheck2 reporter plasmid into our cells of interest. After 48 hours of transfection, we lysed the cells using 1X passive lysis buffer. Subsequently, we performed a luciferase reporter assay using a Promega dual luciferase reporter assay kit. Firefly luciferase activity served as an internal control to normalize the luciferase signal, allowing us to assess the interaction of miRNAs on the regulation of specific target genes.

Invasion assay

To evaluate the effects of miRNAs on cellular invasion, we followed a previously published protocol (*66*). In brief, transwell invasion chambers were coated with 75 µl of a 250 µg/ml collagen IV solution. After 48 hours of miRNA transfection, cells were counted, and 1 x 10^5 cells were re-suspended in 300 µl of 1% serum-containing, antibiotic-free medium. The cells were then added to each transwell chamber, with 750 µl of fetal bovine serum-containing medium in the bottom chamber, creating a gradient that stimulates cell invasion through the collagen IV-coated membrane. Following 6-8 hours of incubation, the invaded cells were stained with crystal violet, and five random fields were captured and counted using ImageJ software.

Gel electrophoresis and immunoblot analysis

Immunoblot assay was performed according to previously published protocols (*67*). After 48 hours of miRNA transfection, cells were harvested and cell lysis was performed using RIPA buffer (50 mM Tris-HCl pH 8.0, 150 mM NaCl, 5 mM EDTA, 0.1% SDS, and 1X protease and phosphatase inhibitor). The protein concentration in the lysates was determined using the Bradford method. Subsequently, 40-100 µg of cell lysates were loaded onto each lane, separated via 4-12% SDS-PAGE, and transferred to a nitrocellulose membrane. To prevent non-specific binding, the membrane was blocked with 5% skim milk and then incubated overnight at 4^0C with primary antibodies targeting

specific proteins, including CD44 (1:1000, Catalog#37259,Cell Signaling Technology), TOP2A(1:500, Catalog#sc-3659, Santa Cruz Biotechnology), ANKRD11(1:1000, Catalog# sc-81049, Santa Cruz Biotechnology), ZBTB4(1:1000, Catalog#sc-514883, Santa Cruz Biotechnology), EPHA4(1:1000, Catalog#sc-365503, Santa Cruz Biotechnology), EHD3(1:1000, Catalog#sc-100723, Santa Cruz Biotechnology), GAPDH(1:2000, Catalog#sc-166545, Santa Cruz Biotechnology), MDM2(1:1000, Catalog#OP115, Sigma Aldrich), RHOC(1:1000, Catalog# 10632-1-AP, Thermo Fisher Scientific), HMGA2(1:1000, Catalog#8179, Cell Signaling Technology), PLAU(1:1000, Catalog# 17968-1-AP, Thermo Fisher Scientific), NUSAP1(1:1000, Catalog#H00051203-B01P). After primary antibody incubation, the membrane was probed with horseradish peroxidase-conjugated secondary antibodies (goat anti-mouse or rabbit) at room temperature for 1 hour. Detection was achieved using a pico-sensitive ECL reagent (Thermo Scientific), and images were captured using an Amersham 600 imager.

Cell proliferation assay

$2X10^4$-$5X10^4$ U87 and U251 cells were seeded and transfected with 30 nM of either scrambled negative control miRNA or primary mimic miR-340, miR-382, or miR-17 inhibitor. After a transfection period of 48 hours, the cells were trypsinized and counted at various time points for seven days. The resulting cell counts were then used to generate growth curves.

RNA isolation, cDNA synthesis, and qPCR

Total RNA was extracted from primary astrocytes, U87, A172, U251, GSC-28 and GSC-34 cells using the Qiagen miRNeasy kit following the manufacturer's protocol. GBM tissue samples were homogenized, and total RNA was isolated using the same kit. Subsequently, 100 ng to 1 µg of total RNA was employed for cDNA synthesis utilizing either the miRscript or miRCURY LNA RT kit. The miRCURY LNA SYBR Green PCR kit was used to assess the expression levels of mature miRNAs. The miRNA fold change was calculated using the delta-delta Ct method, with primary astrocytes used as a control sample to normalize the fold change.

Neurosphere assay

The neurosphere assay was conducted according to a previously published protocol (*66*). Briefly a 6-well plate was initially coated with a poly-ornithine solution and incubated at 37^0C in a tissue culture incubator for one hour. Afterward, the plates were washed twice with 1X PBS. Glioblastoma stem cells GSC-34 and GSC-28 were dissociated and seeded onto the coated plate. Transfection with the scrambled negative control and the primary mimic miR-340, miR-382, and inhibitor against miR-17 was conducted using the Lipofectamine RNAiMax reagent. After 48 hours of transfection, glioblastoma stem cells were dissociated using an accutase solution and cultured in a neurobasal growth medium for another seven days. The number of neurospheres was quantified both manually and also with ImageJ software based on their size classification (large, medium, and small) and represented in a bar graph.

Supplementary Figure Legends

Figure S1: Identification of miRNA targets through PAR-CLIP in glioblastoma cells: A) U87 cells stably expressing Flag-tagged AGO1, AGO2, AGO3 were immunoprecipitated with Flag antibody and immunoblotted with Flag antibody to detect Ago1, Ago2, and Ago3. Supernatant and input were examined to assess pull-down efficiency. The bands at the labeled AGO position show successful pulldown of Ago1, Ago2 and Ago3 respectfully. B) Radiolabeled RNA fragments purified from AGO1, AGO2, AGO3-RNA immuno-complexes were separated on a 15% polyacrylamide gel, and regions of 19-35 bp were excised and purified for 3' and 5' adaptor ligation reactions. C, D) 3' (C) and 5' (D) adaptor ligation reactions were conducted as described in the materials and methods section which shown successful incorporation of adaptors. E) The ligated RNA fragments were reverse transcribed, and libraries were generated for AGO1, AGO2, AGO3 samples. The libraries from AGO1, AGO2, AGO3 were subjected to amplification at different cycles to prevent saturation. F) Heatmaps displaying all the miRNA targets identified in U87 cells by AGO1, AGO2, AGO3 through PAR-CLIP which show that each miRNA exhibits numerous targets across the different AGOs.

Figure S2: Endogenous expression of miR-340, miR-382, and miR-17 in different glioblastoma cell lines and tissues: A,B) Total RNA was extracted from various glioblastoma tissue samples, followed by cDNA synthesis using the Qiagen miScript RT kit. One microgram of RNA was utilized for cDNA synthesis. The cDNA samples were diluted, and RT-qPCR was conducted with miRNA primers against miR-340 (A), miR-382 (B). Normal brain samples were used as controls, and U6 was employed as an internal control for normalization. MiR-340 and miR-382 showed decreased expression compared to normal brain samples. C,D) Different glioblastoma cell lines, including A172, T98G, LN18, U251, U87, SNB19, and patient-derived glioblastoma cell lines (GSC-28, GSC-20, GSC-34, GSC-627, GSC-267) were cultured, and cells were harvested for total RNA isolation using the Qiagen miRNeasy kit. Normal human astrocytes (NHA) were used as normal controls. One microgram of total RNA was used for cDNA synthesis with the miRCURY kit, followed by qPCR with primers against miR-340 (C), miR-382 (D). MiR-340 and miR-382 showed decreased expression compared to normal human astrocytes. E) Total RNA was extracted from different glioblastoma tissue samples followed by cDNA synthesis with miScript RT kit using miR-17 primer set. MiR-17 showed elevated expression in all the glioblastoma tissue samples. F) Expression of miR-17 in various glioma cell lines and patient derived glioma stem cell lines by qPCR. miR-17 showed elevated expressed compared to normal human astrocytes. Results are from three independent experiments. * $P < 0.05$.

Figure S3: Magnetic Resonance-guided Focused Ultrasound (MRgFUS)–microbubbles and brain penetrating nanoparticle (FUS-MB-BPN) mediated delivery of miRNA into mouse brain tumors does not induce toxicity. A) Panel A illustrates the delivery of BPN-conjugated miR-142-3p into the mouse brain using MRgFUS, followed by harvesting of various organs under both FUS and non-FUS conditions, with subsequent H&E staining. B) Panel B presents a table summarizing toxicity assessments by an experienced neuropathologist across different organs Liver, Kidney, Brain, Heart, Spleen, Lung, Lymph nodes, Pancreas which showed there was no apparent off-target toxicity to the organs.

Figure 1

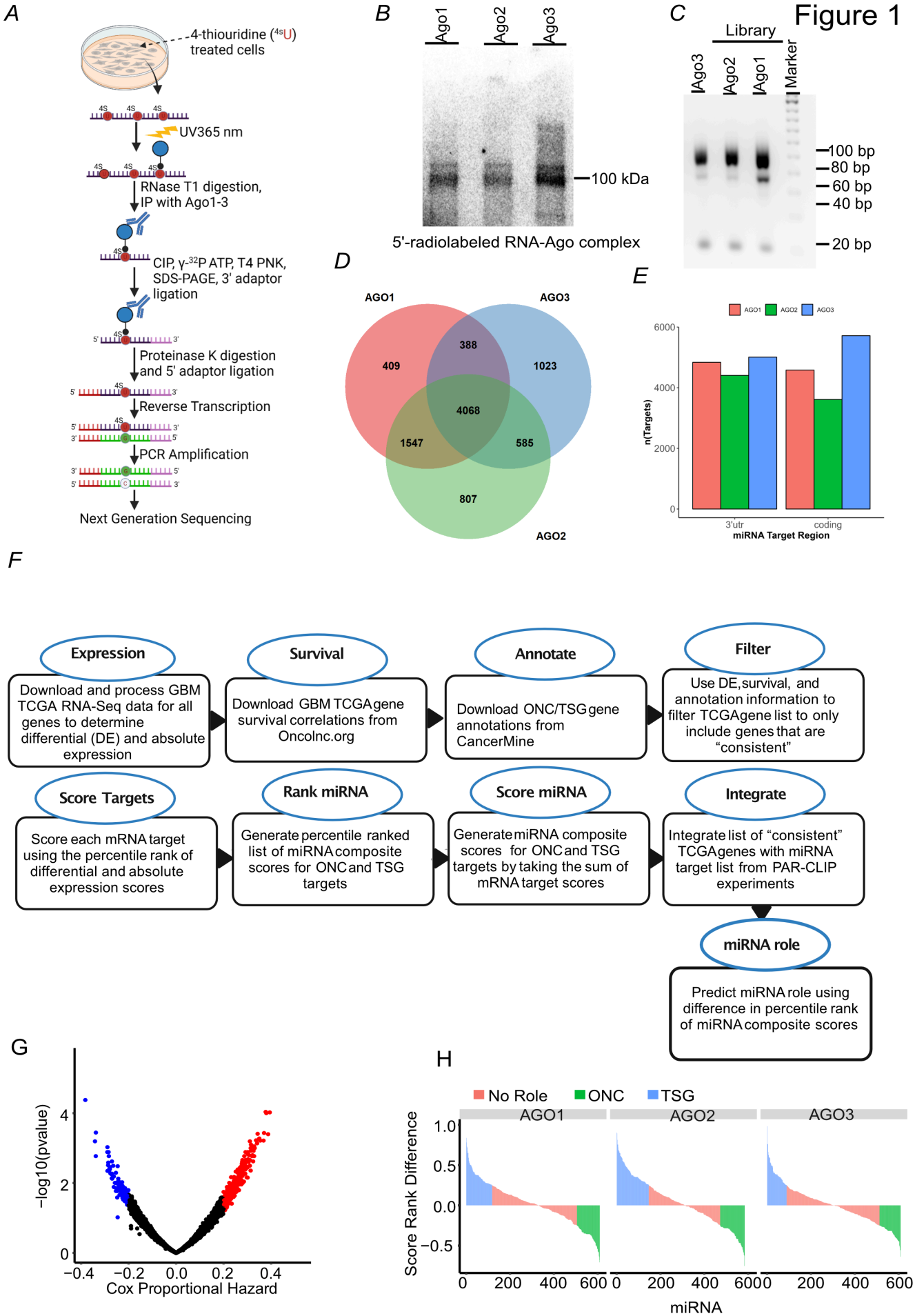

Figure 2

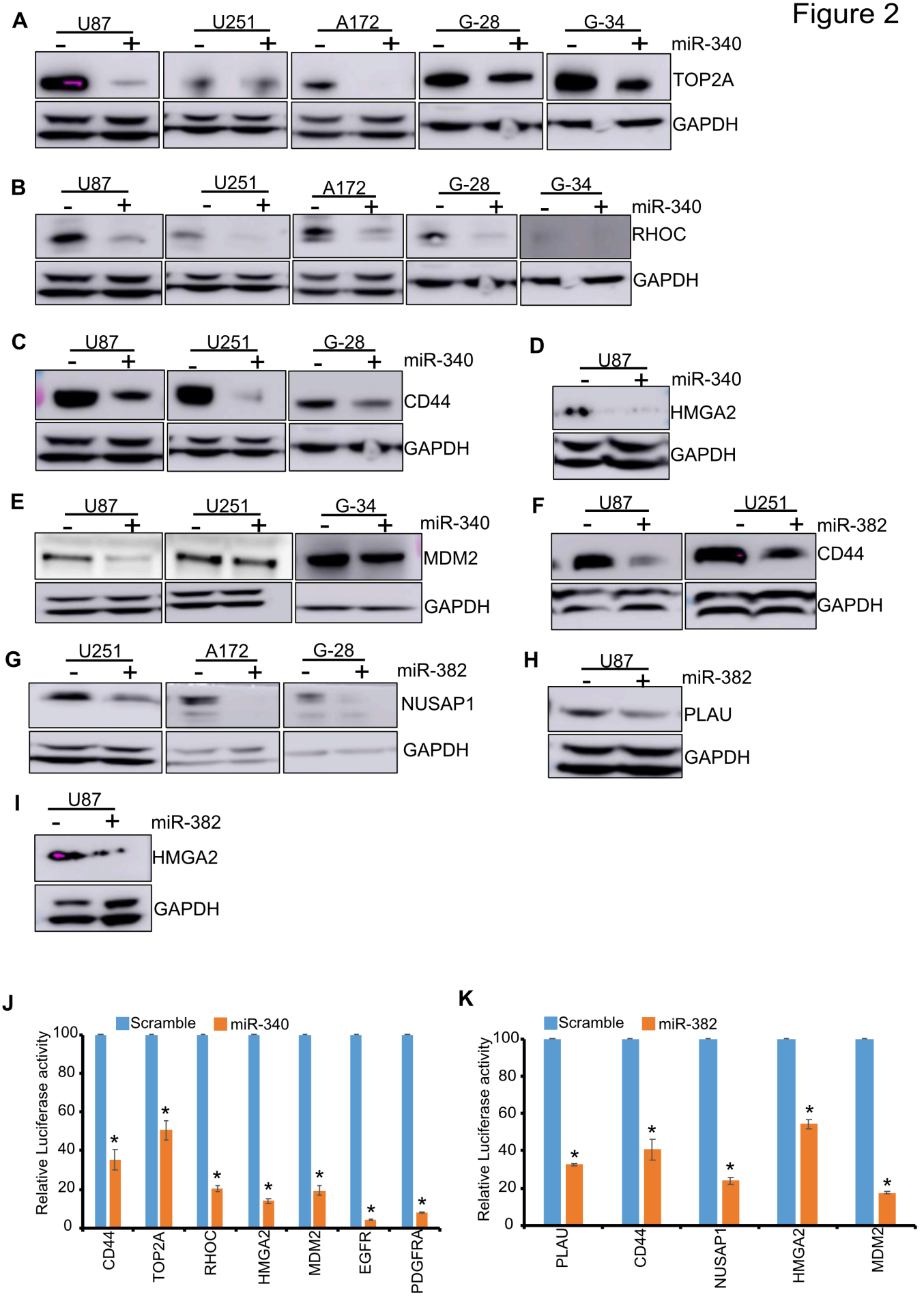

Figure 3

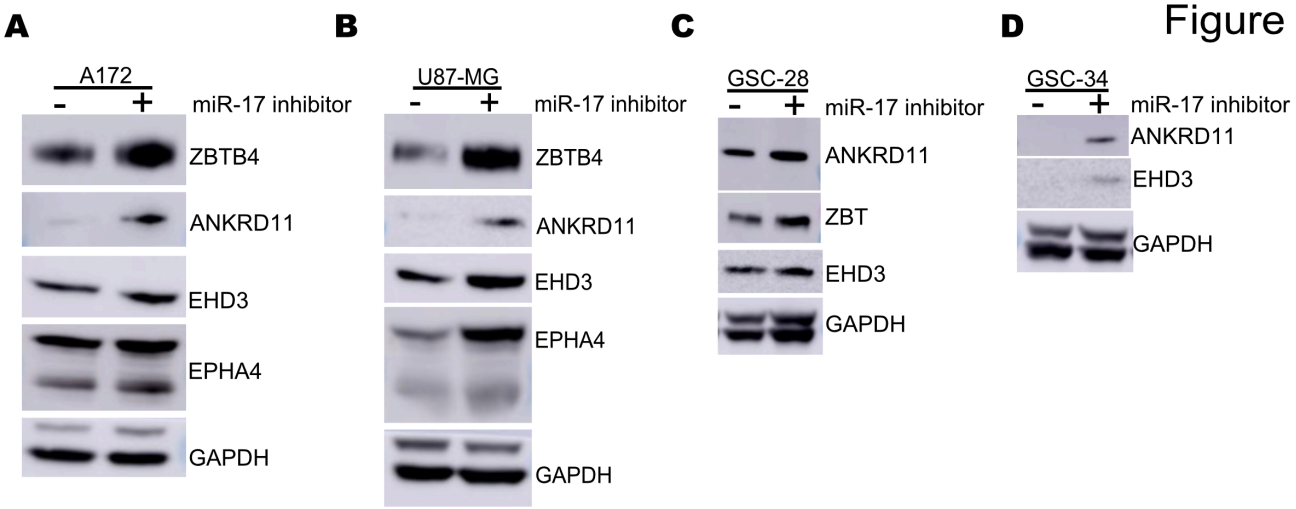

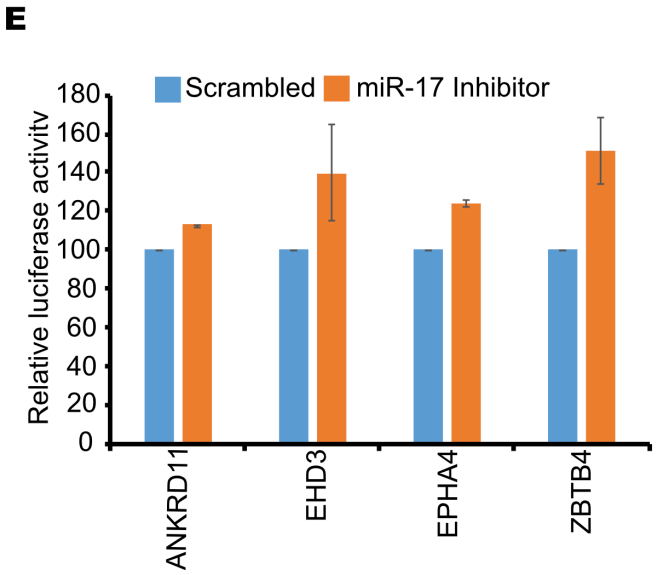

Figure 4

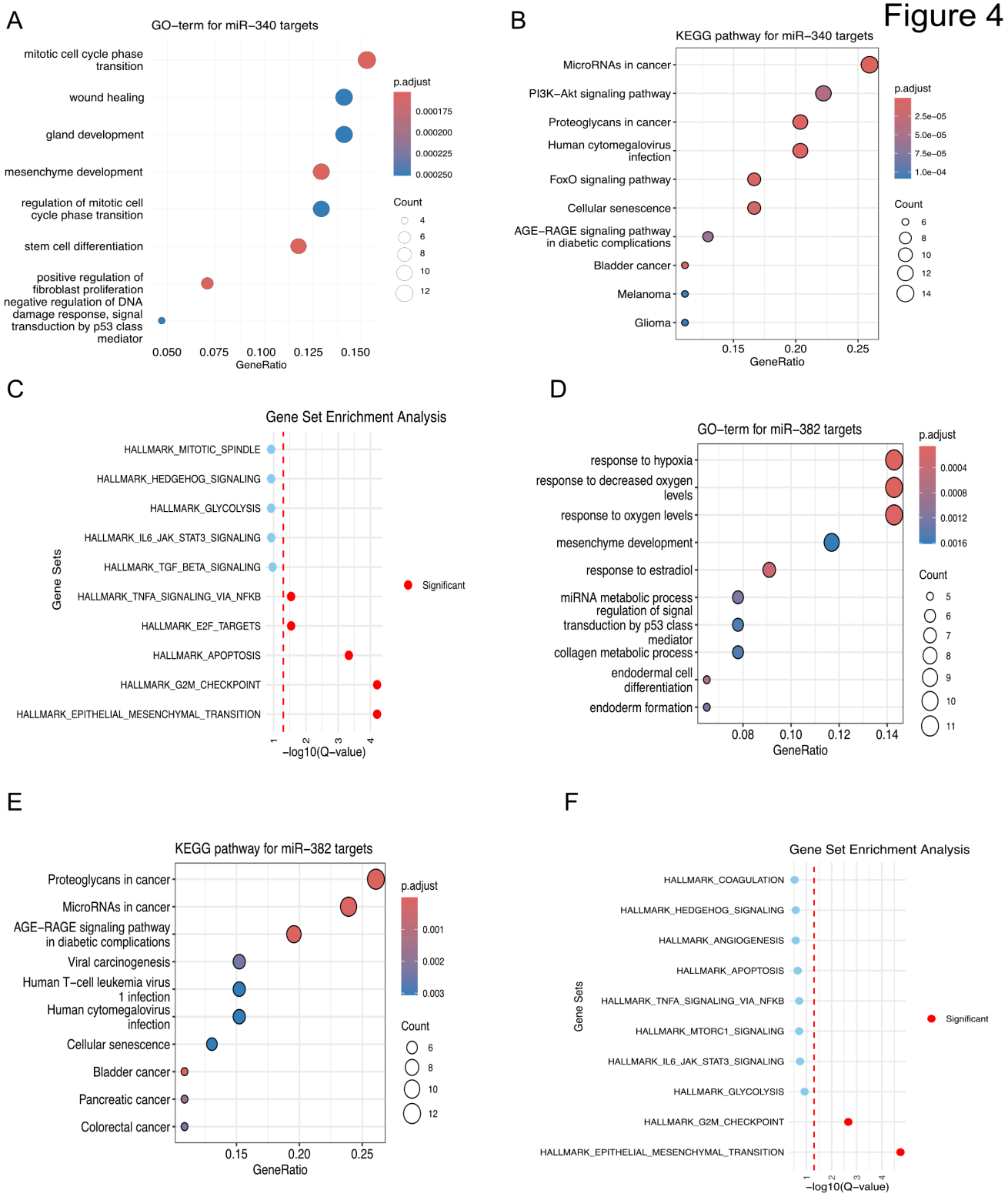

Figure 5

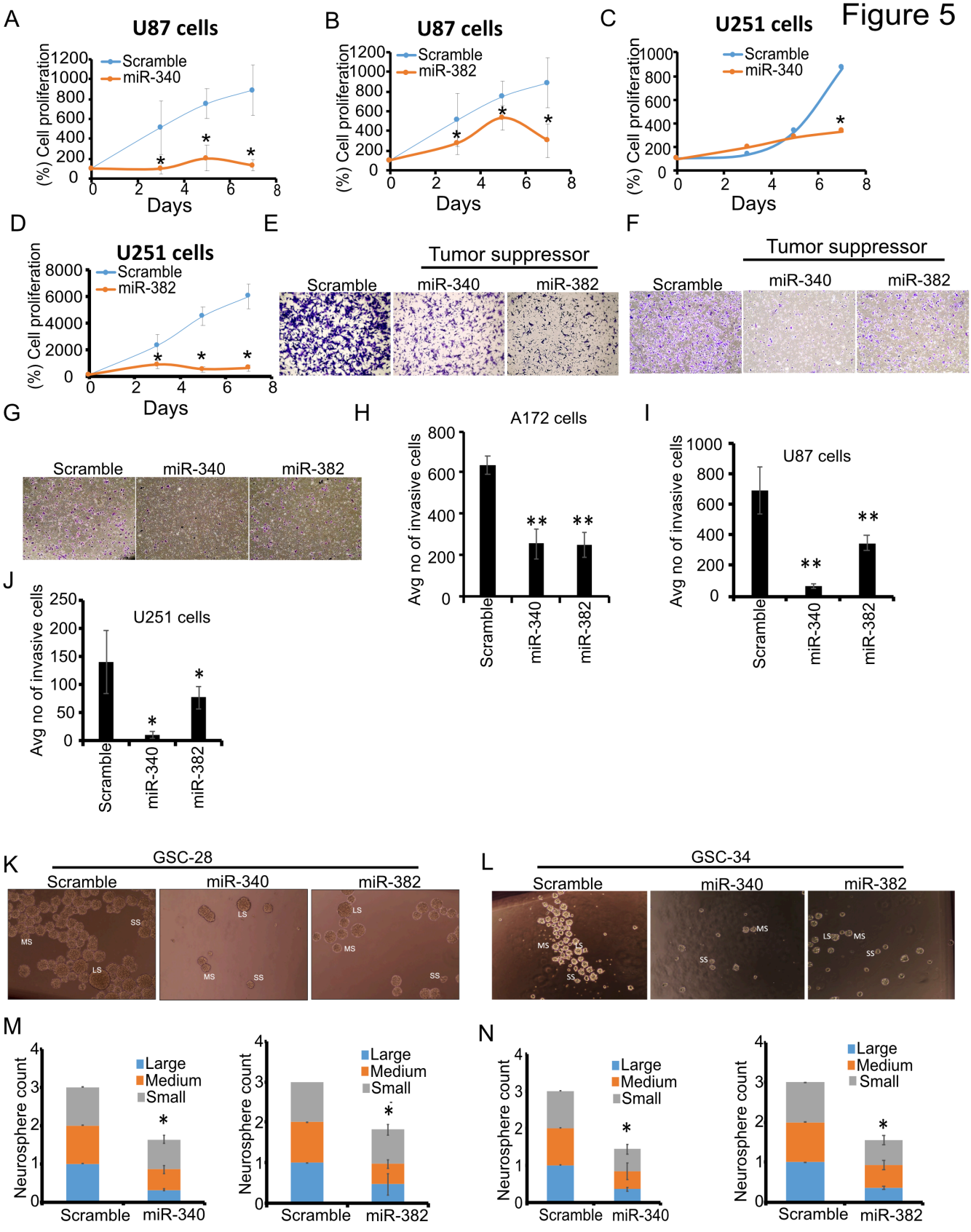

Figure 6

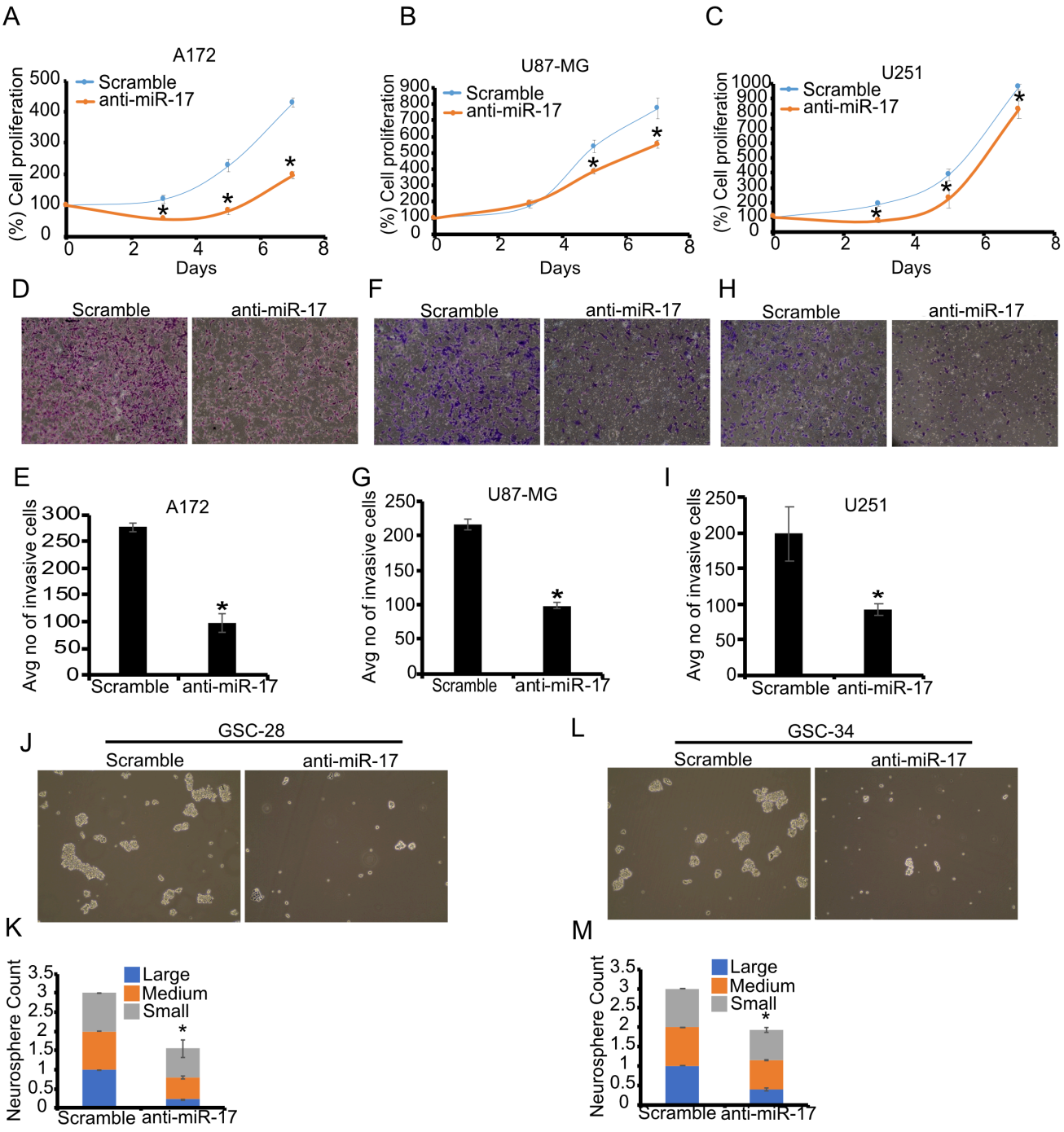

Figure 7

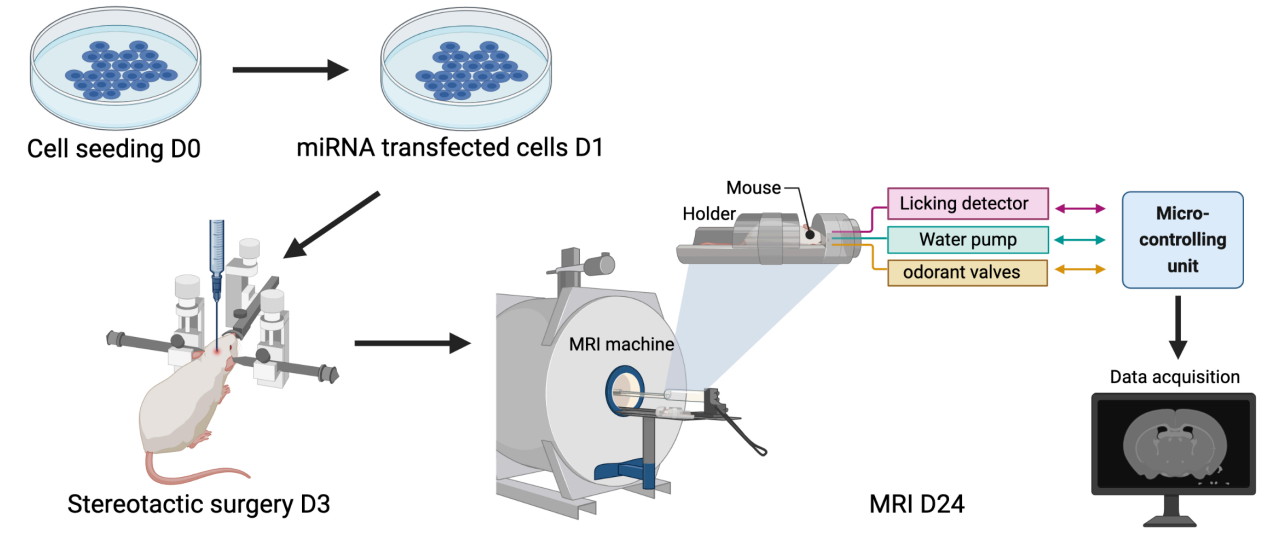

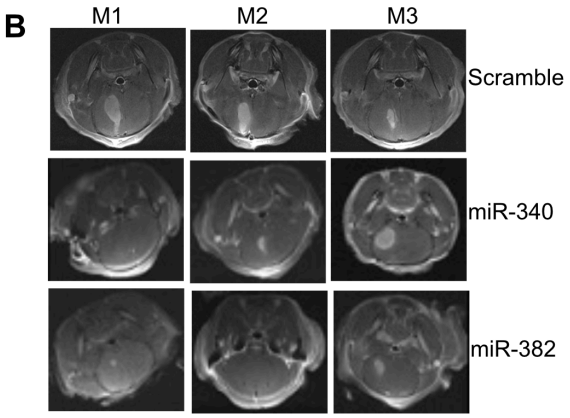

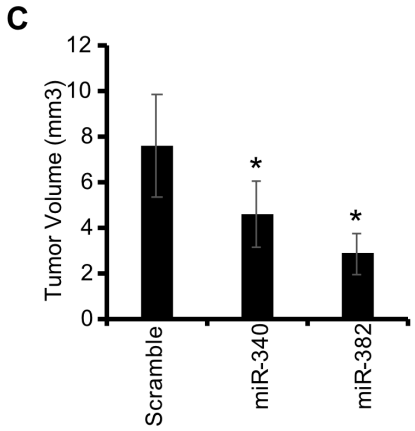

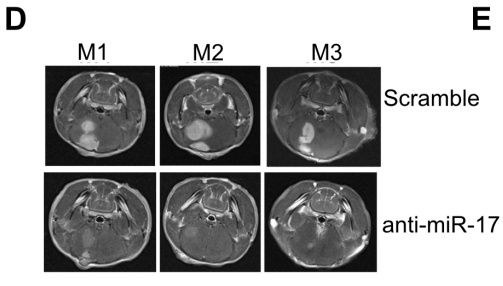

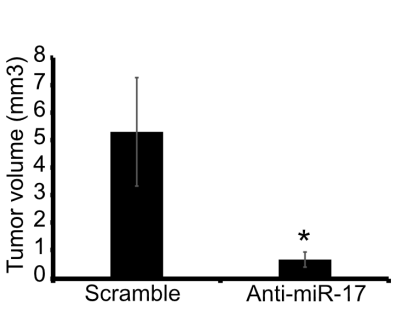

Figure 8

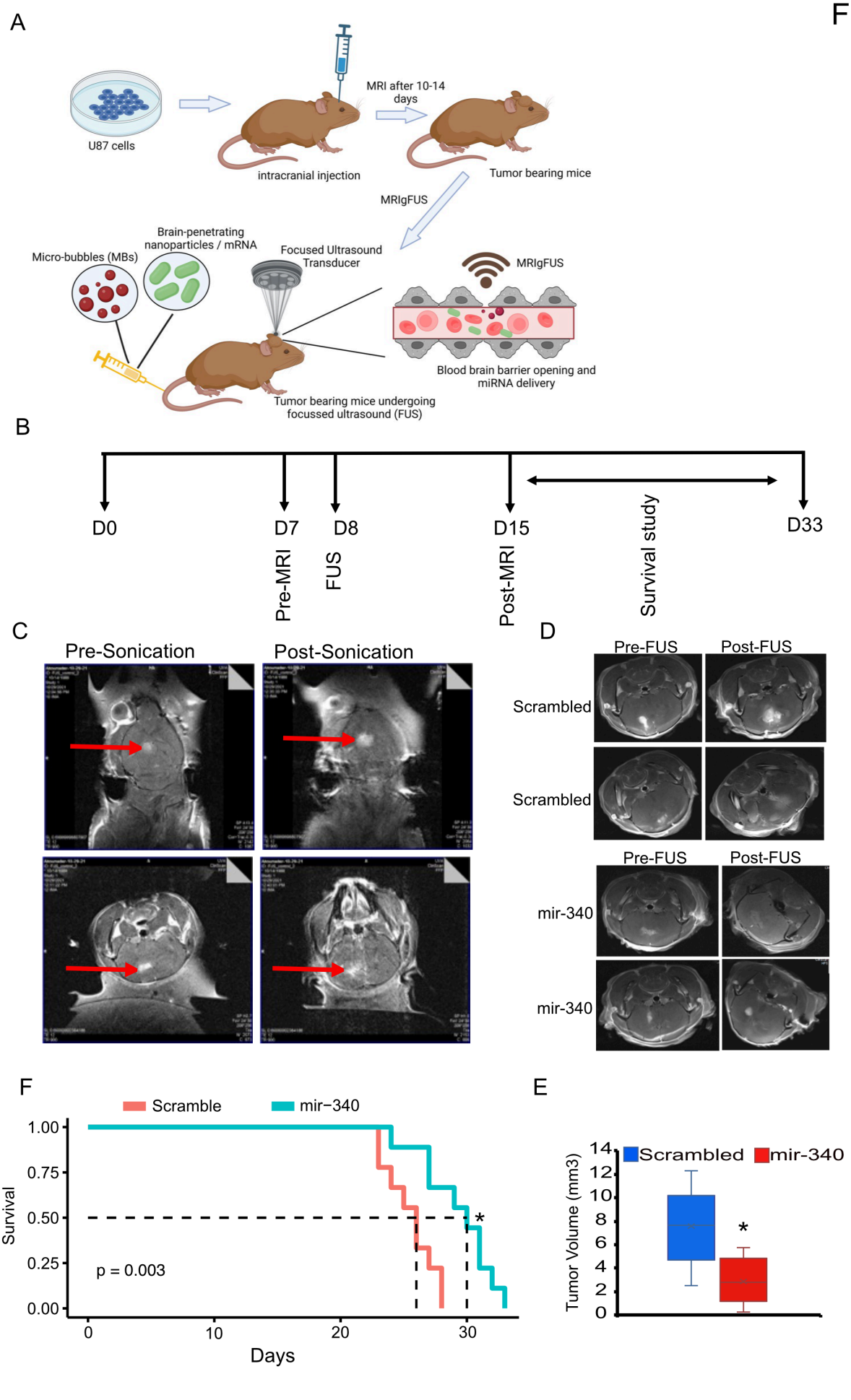

Figure S1

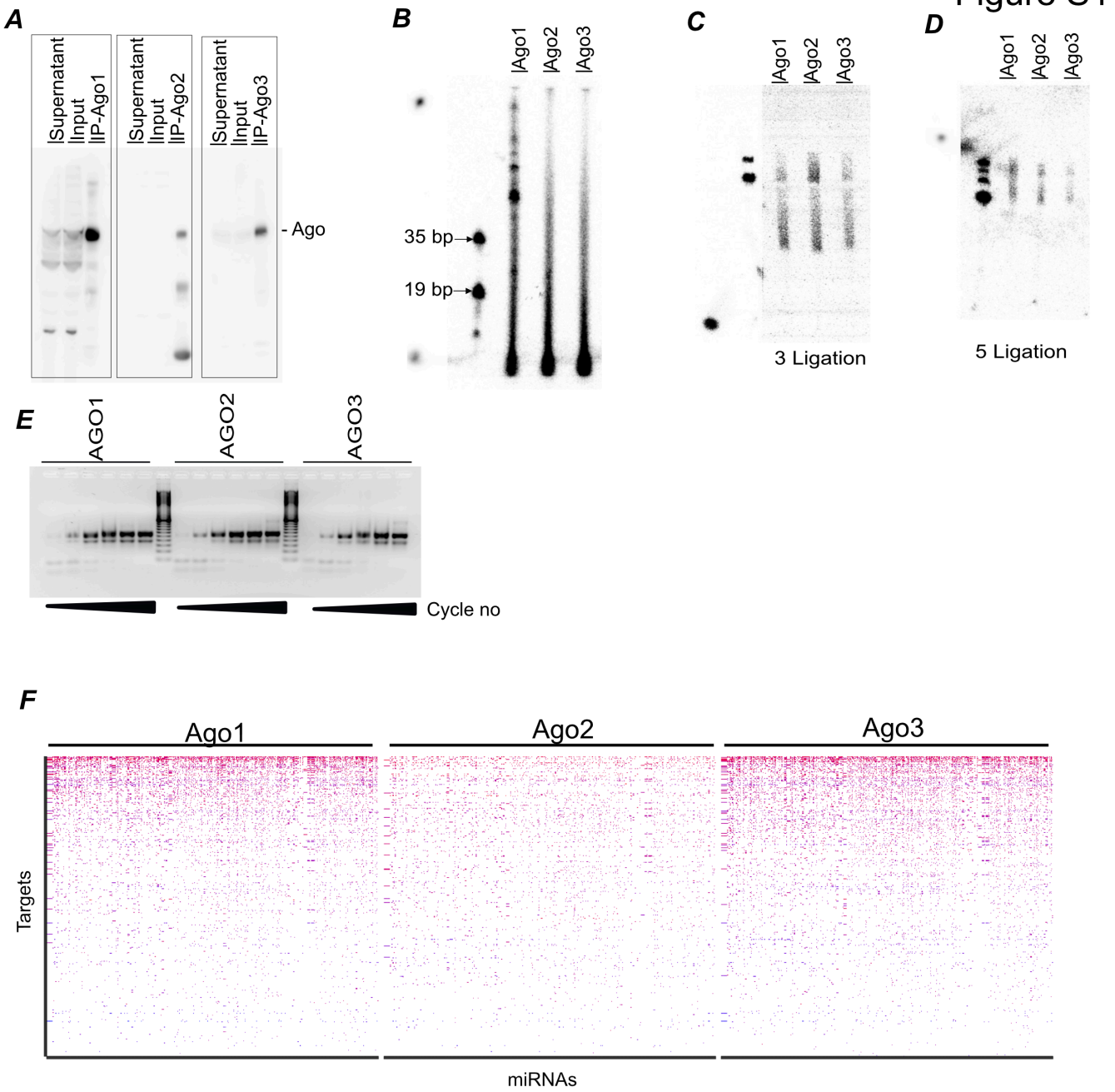

Figure S2

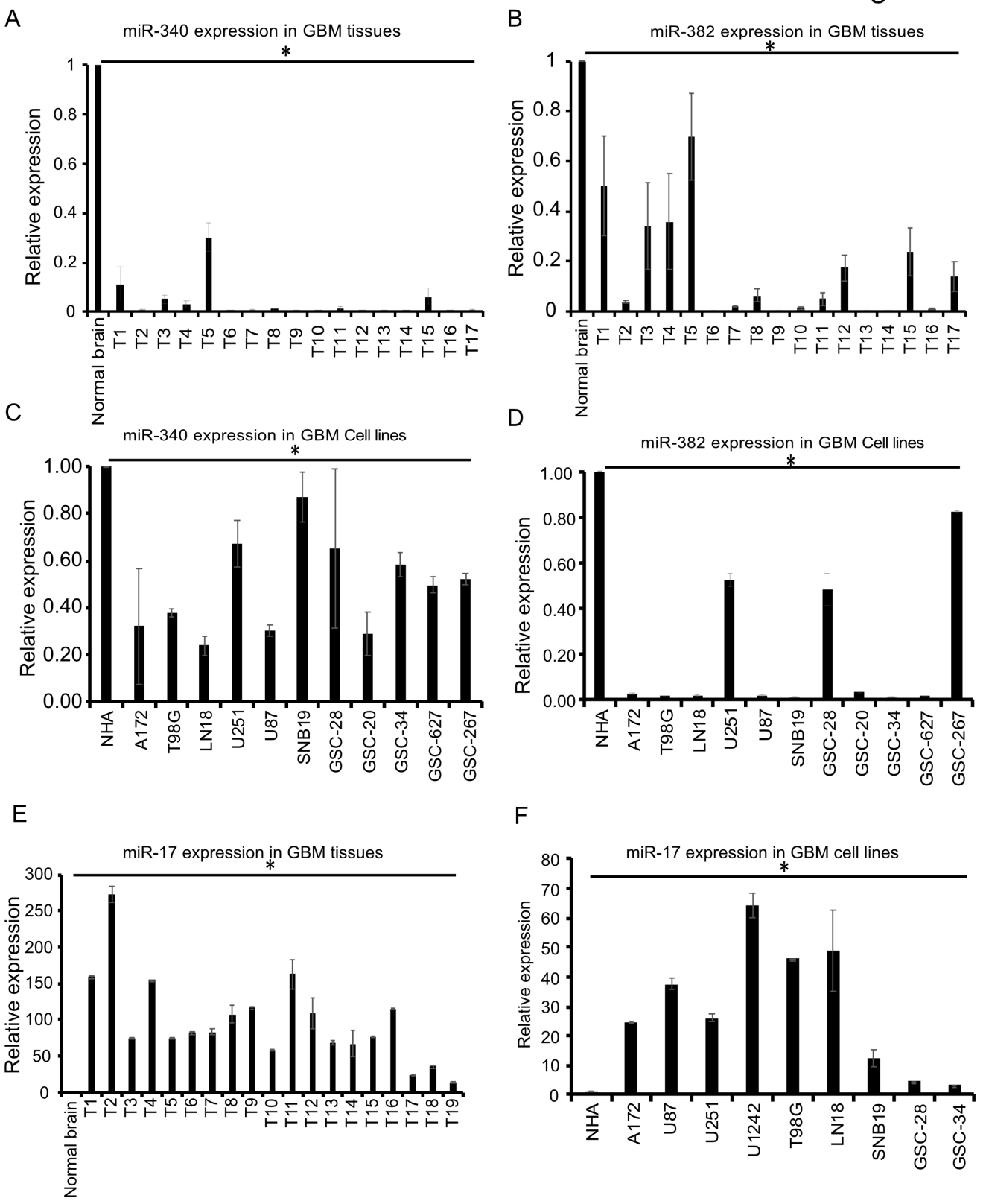

A

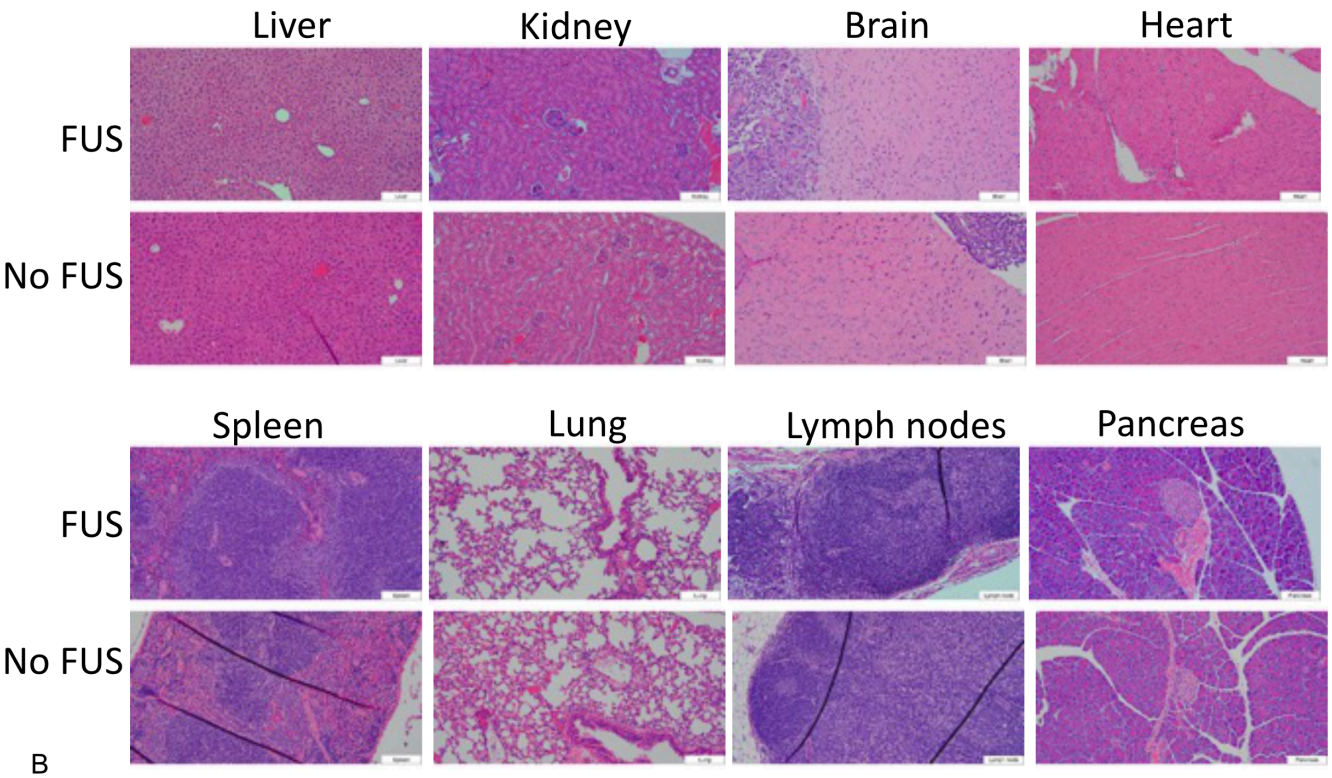

B

Organ	FUS	No FUS
Pancreas	No injury	No injury
Lymph nodes	No injury	No injury
Kidneys	No injury	No injury
Liver	No injury	No injury
Spleen	No injury	No injury
Heart	No injury	No injury
Lungs	No injury	No injury
Brain	Tumor, no injury	Tumor, no injury